THE JOURNAL OF COMPARATIVE NEUROLOGY 422:246–266 (2000)

Rat Somatosensory Cerebropontocerebellar Pathways: Spatial Relationships of the Somatotopic Map of the Primary Somatosensory Cortex Are Preserved in a Three-Dimensional Clustered Pontine Map

TRYGVE B. LEERGAARD,[1] KJERSTI A. LYNGSTAD,[1] JOHN H. THOMPSON,[2] SOFIE TAEYMANS,[3] BART P. VOS,[3] ERIK DE SCHUTTER,[3] JAMES M. BOWER,[2] AND JAN G. BJAALIE[1]*

[1]Department of Anatomy, Institute of Basic Medical Sciences, University of Oslo, N-0317 Oslo, Norway

[2]Division of Biology, California Institute of Technology, Pasadena, California 91125

[3]Born-Bunge Foundation, University of Antwerp, 2610 Antwerp, Belgium

ABSTRACT

In the primary somatosensory cortex (SI), the body surface is mapped in a relatively continuous fashion, with adjacent body regions represented in adjacent cortical domains. In contrast, somatosensory maps found in regions of the cerebellar hemispheres, which are influenced by the SI through a monosynaptic link in the pontine nuclei, are discontinuous ("fractured") in organization. To elucidate this map transformation, the authors studied the organization of the first link in the SI-cerebellar pathway, the SI-pontine projection. After injecting anterograde axonal tracers into electrophysiologically defined parts of the SI, three-dimensional reconstruction and computer-graphic visualization techniques were used to analyze the spatial distribution of labeled fibers. Several target regions in the pontine nuclei were identified for each major body representation. The labeled axons formed sharply delineated clusters that were distributed in an inside-out, shell-like fashion. Upper lip and other perioral representations were located in a central core, whereas extremity and trunk representations were found more externally. The multiple clusters suggest that the pontine nuclei contain several representations of the SI map. Within each representation, the spatial relationships of the SI map are largely preserved. This corticopontine projection pattern is compatible with recently proposed principles for the establishment of subcortical topographic patterns during development. The largely preserved spatial relationships in the pontine somatotopic map also suggest that the transformation from an organized topography in SI to a fractured map in the cerebellum takes place primarily in the mossy fiber pontocerebellar projection. J. Comp. Neurol. 422:246–266, 2000.

Indexing terms: three-dimensional reconstruction; anterograde tracing; cerebellum; corticopontine; electrophysiology; topography

Judging by the number of axons alone, the cerebropontocerebellar pathway is one of the largest pathways in the mammalian brain (Tomasch, 1968, 1969). This pathway, which originates from large parts of the cerebral cortex, reaches almost all regions of the cerebellum (for reviews, see rodal and Bjaalie, 1997; Schmahmann and Pandya, 1997). With this report, we initiate a detailed study in the rat of the projection topography of the pathway that originates in the primary somatosensory cortex (SI) and terminates in the granule cell layer of the cerebellum. The

Grant sponsor: European Community; Grant number: Bio4 CT98-0182; Grant sponsor: Research Council of Norway; Grant sponsor: National Institutes of Health; Grant number: NS37109.

*Correspondence to: Dr. Jan G. Bjaalie, Department of Anatomy, Institute of Basic Medical Sciences, University of Oslo, P.O. Box 1105 Blindern, N-0317 Oslo, Norway. E-mail: j.g.bjaalie@basalmed.uio.no

Received 24 September 1999; Revised 6 January 2000; Accepted 21 February 2000

topography of this pathway is particularly interesting, because it links two brain regions that receive primary somatosensory information that, nevertheless, have very different patterns of somatotopic organization (Bower et al., 1981). Like most regions of the somatosensory system, the body surface is mapped relatively continuously in the SI cortex, that is, with adjacent regions of the body surface generally represented in adjacent parts of the cortex (Woolsey, 1958; Welker, 1971; for review, see Chapin and Lin, 1990). In contrast, the tactile responses in the cerebellar granule cell layer form a highly *discontinuous* or fractured map. Thus, adjacent regions of the body surface are not necessarily represented adjacently within the cerebellum, and a single body region typically maps onto multiple cerebellar locations (Shambes et al., 1978; Bower and Kassel, 1990; for review, see Welker, 1987).

Physiological data indicate that the tactile-related cerebrocerebellar circuit exhibits a precise projection pattern with regions of SI influencing only those regions of the cerebellum with which they share a receptive field (Bower et al., 1981). Little is known, however, about the structural basis of this transformation from a continuous to a fractured sensory map. Such knowledge is relevant not only for the understanding of cerebrocerebellar circuits but also for understanding brain-map transformations in general. Previous investigations have suggested general somatotopic patterns in the projection from SI to the pontine nuclei (Brodal, 1968, 1978; Burne et al., 1978; Mihailoff et al., 1978, 1984, 1985; Wiesendanger and Wiesendanger, 1982; Kosinski et al., 1986, 1988; Lee and Mihailoff, 1990; Panto et al., 1995; for review, see Brodal and Bjaalie, 1997). However, these studies do not make it clear whether the pontine somatotopic map is organized in a continuous, fractured, or some other fashion.

In this paper, we focus on the first link in the pathway to the cerebellum: the SI projection to the pontine nuclei. We have used electrophysiological mapping procedures to define the locations within SI of the perioral region, upper lip, forelimb, trunk, and hindlimb regions. Following this mapping, anterograde axonal tracers were injected into the electrophysiologically identified locations, and computerized, three-dimensional (3-D) reconstruction techniques were used to examine the complex labeling patterns in the pontine nuclei. We report a projection pattern with several, separated terminal fields of SI axons for each body representation. The terminal fields are confined to lamellar subspaces and are distributed in accordance with topographic patterns of development of the pontine nuclei (Leergaard et al., 1995). Considering the complicated, fractured organization found in cerebellar maps, the spatial relationships of the pontine somatotopic map are relatively simple and largely reproduce the continuity of SI somatotopic map. We discuss this organization and its possible implications for functions of the pontine nuclei and the further information transfer to the cerebellum. Preliminary results have been presented elsewhere in abstract form (Lyngstad et al., 1996).

MATERIALS AND METHODS

Surgical procedures and electrophysiological mapping

A total of 25 adult female Sprague Dawley rats (Simonsen Laboratories, Gilroy, CA; IFFA CREDO, Brussels, Belgium) were used in this study (Table 1). All animal procedures were reviewed by the local institutional animal welfare committee and were in compliance with National Institutes of Health guidelines for the use and care of laboratory animals. The animals were anesthetized with a mixture of 25% ketamine hydrochloride (100 mg/ml), 6.3% xylazine (20 mg/ml), and 0.25% acepromazine maleate (10 mg/ml) in physiological saline. An initial intramuscular injection of 0.20–0.25 ml/kg of this mixture was followed by an intraperitoneal injection of sodium pentobarbital (50 mg/ml; 0.05–0.06 ml/kg). Anesthetic depth was monitored by eye-blink reflex, respiratory frequency, and response to toe pinch. Supplementary intramuscular injections of the drug mixture (one-third of the initial dose) were given every 2 hours after the first injection. The animal was placed on a heating pad with rectal temperature feedback to maintain stable body temperature. The head was positioned and immobilized in a stereotaxic frame. The somatosensory cortex was exposed, and, after incision of the dura, the opening of the dura was filled with lukewarm gel foam or saline.

TABLE 1. Experimental Material: Tracers and Location and Size of Injection Sites[1]

Animal no.	Tracer	Injection site	Size of injection site (μm)	3D reconstruction
R101	WGA-HRP	Total SI	500–1,100	+
R102	BDA	Total SI	300–1,400	+
R103	WGA-HRP	Perioral	750–1,250	+
R104	WGA-HRP	Upper lip	550	+
R105	WGA-HRP	Upper lip	580	+
R106	Pha-1	Upper lip	1,100	+
R107	Pha-1	Upper lip	900	+
R108	Pha-1	Upper lip	1,250	+
R109	Pha-1	Upper lip	1,250	+
R110	Pha-1	Upper lip	950	+
R111	Pha-1	Upper lip	800	—
R112	Pha-1	Upper lip	1,100	—
R113	BDA	Upper lip	700	+
R114	BDA	Forelimb	450	+
R115	BDA	Forelimb	700	+
R116	BDA	Forelimb	1,300	+
R117	BDA	Forelimb	350	+
R118	BDA	Trunk	900	+
R119	BDA	Trunk	340	+
R120	BDA	Trunk	550	+
R121	BDA	Trunk	300	+
R122	BDA	Hindlimb	300	—
R123	BDA	Hindlimb	1,250	+
R124	BDA	Hindlimb	500	+
R125	BDA	Hindlimb	200	+

[1]3D, three-dimensional; WGA-HRP, wheat germ agglutinin-horseradish peroxidase; SI, primary somatosensory cortex; BDA, biotinylated dextran amine; Pha-1, *Phaseolus vulgaris*-leucoagglutinin.

A video image of the exposed area was digitized and visualized by using customized software on a Silicon Graphics workstation (Silicon Graphics, Inc., Mountain View, CA; Fig. 1A). Extracellular recordings of SI body surface responses were made with either glass micropipettes filled with 2 M NaCl (10 μm diameter; 1 MΩ impedance) or tungsten microelectrodes (1 μm tip diameter; 2 MΩ impedance; World Precision Instruments, Hertfordshire, England) connected to an amplifier and a loudspeaker set-up. The electrode was inserted perpendicular to the cortical surface and was advanced slowly to layers IV–V (800–1,200 μm below the pial surface) with a micromanipulator.

The skin was tapped gently and stroked with a handheld wooden rod, and multiunit activity was determined audibly. The body region that, when stimulated, elicited the strongest response identified the position in the corti-

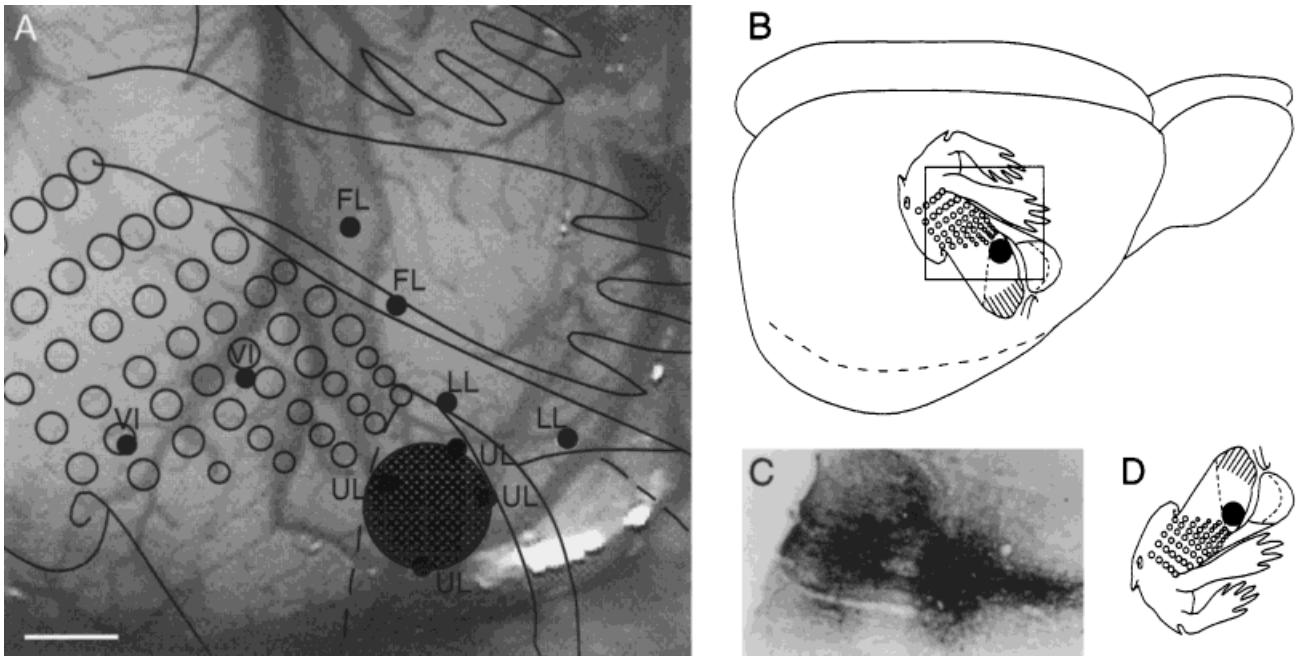

Fig. 1. **A:** Videoimage of the exposed right primary somatosensory cortex (SI) of animal R113. Electrode recording positions are indicated by black dots. This animal was injected with biotinylated dextran amine (BDA) into the electrophysiologically defined upper lip representation. The cross-hatched circle shows the extent of the BDA injection site at the level of cortical layer V. The SI somatotopic map (redrawn from Fig. 3 in Welker, 1971) is superimposed on the videoimage and is matched in position with the electrophysiological recording sites. **B:** Line drawing (modified from Welker, 1971) of the right cerebral hemisphere with the SI somatotopic map. The black area indicates the position and size of the injection site. The frame shows the extent of the videoimage in A. **C:** Photomicrograph of a frontal section through the center of the BDA injection site. **D:** A mirrored and rotated image of the SI somatotopic map that is used in subsequent figures. This orientation of the map facilitates comparisons with the pontine somatotopic map. FL, forelimb; LL, lower lip; UL, upper lip; VI, vibrissae. Scale bar = 500 μm in A (also applies to C).

cal somatosensory map. A video image for each electrode penetration was superimposed on the digitized image of the brain surface, thus allowing direct registration of the exact location of each penetration together with information about the body part(s) generating the response (Fig. 1A). Depending on the position within SI, about 10–30 sites were mapped in each experiment. In eight experiments, single-unit recordings were made. Once the receptive field of these units was determined by using the hand-held wooden rod, a standardized mechanical tap stimulus (10 msec) was applied to its center by using a stainless-steel probe (1 mm diameter; flat surface; maximal excursion, 2.5 mm) that was mounted on an electromagnetic activator and driven by a Grass 11S digital stimulator. The stimulation paradigm started with 50 trials without stimulation, followed by 100 trials with stimulation, and then 50 trials without stimulation. Stimuli were delivered at 0.5 Hz. Peristimulus time histograms were calculated to quantify the evoked responses. Spike train analyses were performed by using NeuroExplorer (Nex Technologies, Winston-Salem, NC). This additional method quantified the synchrony of the single-unit response with the stimulus. The results confirmed the audibly determined multiunit responses in all eight cases.

Tracer injections and histochemistry

After electrophysiological mapping, neuronal tracers were injected iontophoretically into defined parts of the SI based on the receptive field maps. Each injection site was positioned accurately in relation to the electrode recording positions in the digitized image of the brain surface (Fig. 1A).

Four rats were injected with 2.5% wheat germ agglutinin-horseradish peroxidase (WGA-HRP; Sigma, St. Louis, MO), seven rats were injected with 2.5% *Phaseolus vulgaris*-leucoagglutinin (Pha-l; Vector Laboratories, Burlingame, CA), and 14 rats were injected with 10% biotinylated dextran amine (BDA; Molecular Probes, Eugene, OR). The tracers were injected iontophoretically through a glass micropipette (10–40 μm in diameter). For each injection, a pulsed, 5-μA current (duty cycle, 5 seconds) was used between 5 minutes and 30 minutes. To avoid backflow of the tracer, the micropipette was left in situ for a few minutes prior to retraction.

After a survival period of 3 days (WGA-HRP-injected animals) or 1 week (Pha-l- and BDA-injected animals), the rats were reanesthetized and perfused transcardially with warm physiological saline, warm fixative (see below), and finally cold 10% sucrose. All solutions were prepared in 0.1 M phosphate buffer, pH 7.4. For a fixative, the WGA-HRP-injected animals received a mixture of 1% paraformaldehyde and 1.25% glutaraldehyde, whereas the Pha-l- and BDA-injected animals received 4% paraformaldehyde. The brains were removed, photographed, and soaked in 30% sucrose for 1–4 days prior to sectioning. Frontal sections of the cerebral cortex and transverse sections of the brainstem were cut at 50 μm on a freezing microtome. Every second section through the injection site in the

cerebral cortex and complete series of sections through the pontine nuclei were processed histochemically. In WGA-HRP-injected cases, sections were treated with tetramethylbenzidine (TMB) according to Mesulam (1982). In Pha-l-injected cases, sections were processed as outlined by Gerfen and Sawchenko (1984). Sections from the BDA-injected cases were processed according to steps 1–7 in Lanciego and Wouterlood (1994). For both Pha-l and BDA processing, the avidin-biotin solution (as used in the original protocols) was substituted with the streptavidin-biotinylated horseradish-peroxidase complex (Amersham International, Buckinghamshire, England), as employed by Lehre et al. (1995).

Digitization, 3-D reconstruction, and data analysis

The distribution of labeled axons within the pontine nuclei and several reference lines were recorded by using an image-combining, computerized microscope system based on the Leica Medilux and DMR microscopes (Leica, Deerfield, IL). Details on software and technical solutions are reported in Leergaard and Bjaalie (1995). Complete series of sections through the pontine nuclei were digitized by using a ×25 lens. The ventral surface of the pons, the outlines of the pontine gray, the contours of the corticobulbar and corticospinal fiber tract (referred to below as the peduncle), the midline, and the fourth ventricle were coded as lines and served as fiducial marks. The plexuses of BDA- or Pha-l-labeled axons within the pontine gray were coded semiquantitatively as points (see also Leergaard and Bjaalie, 1995; Leergaard et al., 1995). In areas with a low density of labeling, point coordinates were placed at regular intervals along the length of single axons. In areas with dense labeling, it was impossible to assign coordinates to individual fibers. Then, a rough correspondence was sought between the density of labeling and the number of digitized points, resulting in tight point clusters corresponding to dense axonal plexuses (compare Fig. 2B with Fig. 2C). Similarly, in the WGA-HRP-injected animals, the putative terminal fields were point coded with a density of point coordinates roughly corresponding to the density of TMB granules.

For 3-D visualization and analysis of the distribution of labeling, we used the software program Micro3D for Silicon Graphics workstations (version 1.0; Oslo Research Park, Oslo, Norway), which was developed at the Neural Systems and Graphics Computing Laboratory, University of Oslo (http://www.nesys.uio.no/). The forerunners of this software have been used in several recent investigations (Leergaard et al., 1995; Malmierca et al., 1995, 1998; Bjaalie et al., 1997a,b; Berg et al., 1998; Bajo et al., 1999, Vassbø et al., 1999). The digitized sections were aligned interactively on the screen with the aid of the reference lines (see above). Each section was assigned a z-value defined by its thickness and serial number. Tissue shrinkage was estimated by comparing drawings of sections before and after the histochemical processing. To maintain correct in vivo proportions in the 3-D reconstructions, section thickness, which originally was 50 μm,) was set at 40 μm in TMB-incubated sections and at 45 μm in sections that were processed for Pha-l and BDA as an adjustment for a linear shrinkage of approximately 20% and 10%, respectively. To facilitate the alignment, real-time rotation with inspection of the 3-D reconstructions from different angles of view was used. The reconstructions (essentially consisting of point and line coordinates) served as a basis for the further visualization and analyses of densities and distribution of point clusters (Figs. 4–6, 13). Density maps were produced by dividing a particular projection into squares of 5 × 5 μm by using a grid. Each square was assigned a gray level corresponding to the density of dots within a radius of 100 μm centered on the square (Fig. 7). Surface modeling was performed either with a simple triangulation method by using the software library SISL (SINTEF Spline Library; cf. Bjaalie et al., 1997a) or the software program Nuages (Geiger, 1993). Surfaces were used to demonstrate the boundaries of the pontine nuclei, the ventral surface of the brainstem, and the descending fiber tracts (Figs. 4–6). Surface modeling also was used to illustrate the shape and size of the point clusters. To determine the location of the contour lines that were used as the basis for this surface modeling, the point coordinates were visualized as large dots. Thereby, the continuous regions of labeling were identified. These regions were then outlined interactively in each section for each body representation. Thus, the regions with the lowest densities, which, typically, were located at the periphery of the major clusters or at some distance from the clusters, were excluded. This procedure lead to the inclusion of >90% of all points within the surfaces.

Illustrations were assembled with Showcase software (Silicon Graphics Inc.). Photomicrographs of sections were taken through a Leica DMR microscope (Figs. 1C, 3C–H, 11A) or through a Nikon Multiphot microscope (Nikon, Tokyo, Japan) equipped with a MacroNIKKOR 1:4.5 lens (Figs. 2A,B, 3A,B).

RESULTS

Injection sites

The size of each injection site (Table 1) was defined by the maximum width of dense staining at the level of layer V (the cortical layer containing cell bodies of corticopontine neurons). All injections were restricted to the gray matter except in one case (see below). Photomicrographs of representative injection sites are shown in Figures 1 and 2.

Twenty-two animals received *single injections* into the electrophysiologically defined SI representations of either the upper lip, the proximal forelimb, the distal forelimb, the trunk, the proximal hindlimb, or the distal hindlimb. Three animals received *multiple injections* of a single tracer into SI. One of these received five injections into the electrophysiologically defined perioral area of SI. Two received injections throughout SI (10 injections in one case, and 20 injections in the other case).

Terminology

The term pontine nuclei is used here to include the gray matter that partly embraces the descending fiber tract (corticobulbar and corticospinal fibers, referred to below as the *peduncle*) and the medial lemniscus (Figs. 3A,B, 4). We do not include the dorsally located nucleus reticularis tegmenti pontis, which is organized differently with respect to cytoarchitecture and connectivity (Mihailoff et al., 1981; Torigoe et al. 1986; however, see also Schwarz and Thier, 1996). Furthermore, we do not subdivide the pontine gray (see, e.g., Mihailoff et al., 1981), because there is no apparent correlation between these subdivisions on the

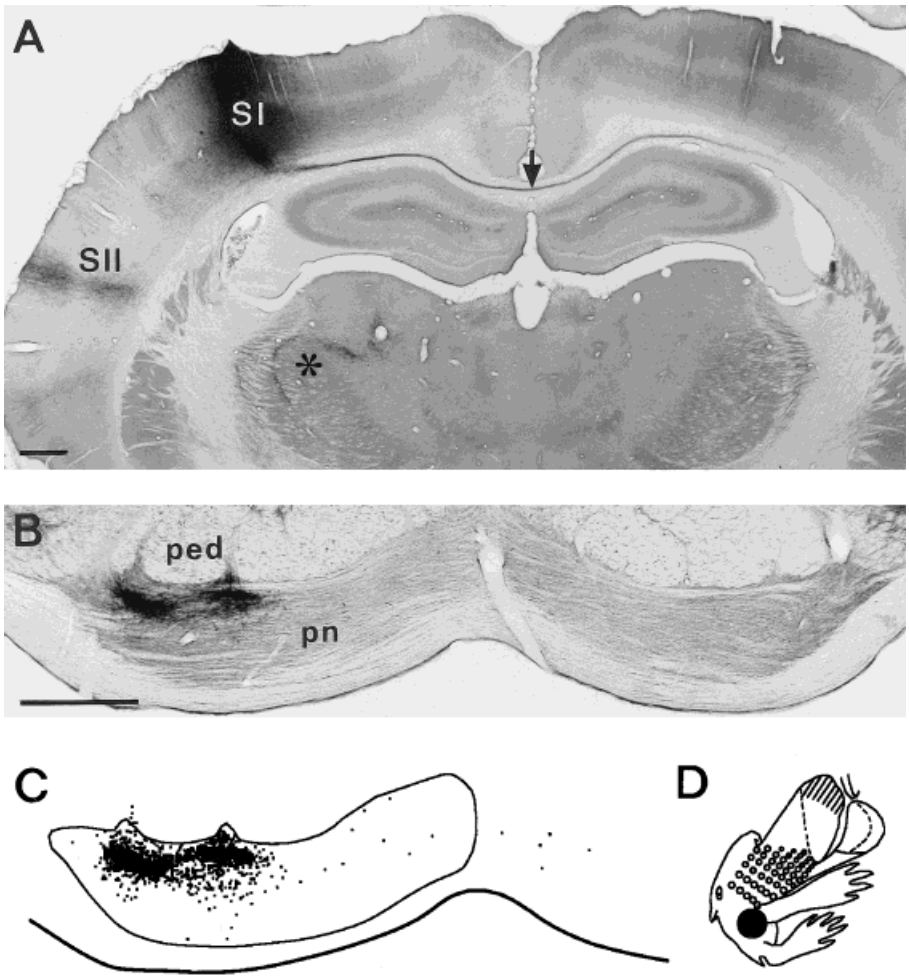

Fig. 2. **A:** Photomicrograph of a frontal section through the center of the BDA injection site in the right SI trunk representation in case R118 (the same case is shown in Figs. 5, 6). The arrow indicates a bundle of labeled callosal fibers. Labeling also is visible in the secondary somatosensory cortex (SII; cf. Koralek et al., 1990). The sickle-shaped labeling in the posterior complex of the thalamus (asterisk) is in accordance with the corticothalamic somatotopy described by Fabri and Burton (1991). **B:** Photomicrograph of a transverse section through the midpontine level in the same case showing two dense plexuses of BDA-labeled fibers dorsolaterally, close to the descending peduncle. **C:** Computerized plot of the same section shown in B. The thick contour line represents the ventral surface of the pons, and the thin contour line represents the boundaries of the gray matter. Dots represent the distribution of labeled axons in the pontine nuclei. **D:** Standard somatotopic map of SI used to show the position and size of the BDA injection site in this case. SI, primary somatosensory cortex; SII, secondary somatosensory cortex; ped, peduncle; pn, pontine nuclei. Scale bars = 500 μm in A,B (bar in B also applies to C).

one hand and the afferent and efferent connections on the other hand (for a review, see Brodal, 1987; see also Wiesendanger and Wiesendanger, 1982; Mihailoff et al., 1985; current study).

In this report, we use terminology in which the *internal* region of the pontine nuclei is defined as a centrally located core close to the peduncle. Regions located outside this core (that is, medial, lateral, ventral, caudal, or rostral to it) are referred to as *external*. This terminology was used previously to describe the establishment of topographic patterns during development in the pontine nuclei of rats (Leergaard et al., 1995; see also Altman and Bayer, 1978, 1987) and proved useful also for the current analyses.

General features of pontine labeling

Three tracers were used in this investigation. In nine animals, the electrophysiologically identified upper lip representation of SI was injected with either WGA-HRP, Pha-l, or BDA (Table 1), and the properties of the three tracers were compared. We observed that BDA and Pha-l gave rise to identical labeling patterns in the pontine nuclei (see below). Labeling with WGA-HRP was located in the same parts of the pontine nuclei but generally was more restricted than the labeling found after injections of the same size with BDA or Pha-l. Finally, in our hands, histochemical processing for BDA was faster than processing for Pha-l. For these reasons, we selected BDA as our main tracer in this investigation.

The three tracers produced anterograde labeling in the pontine nuclei with different characteristics. In cases injected with WGA-HRP, the TMB reaction product appeared as granules. It is generally assumed that anterograde labeling with WGA-HRP outlines terminal fields of axons (Mesulam, 1982). Pha-l and BDA both labeled the

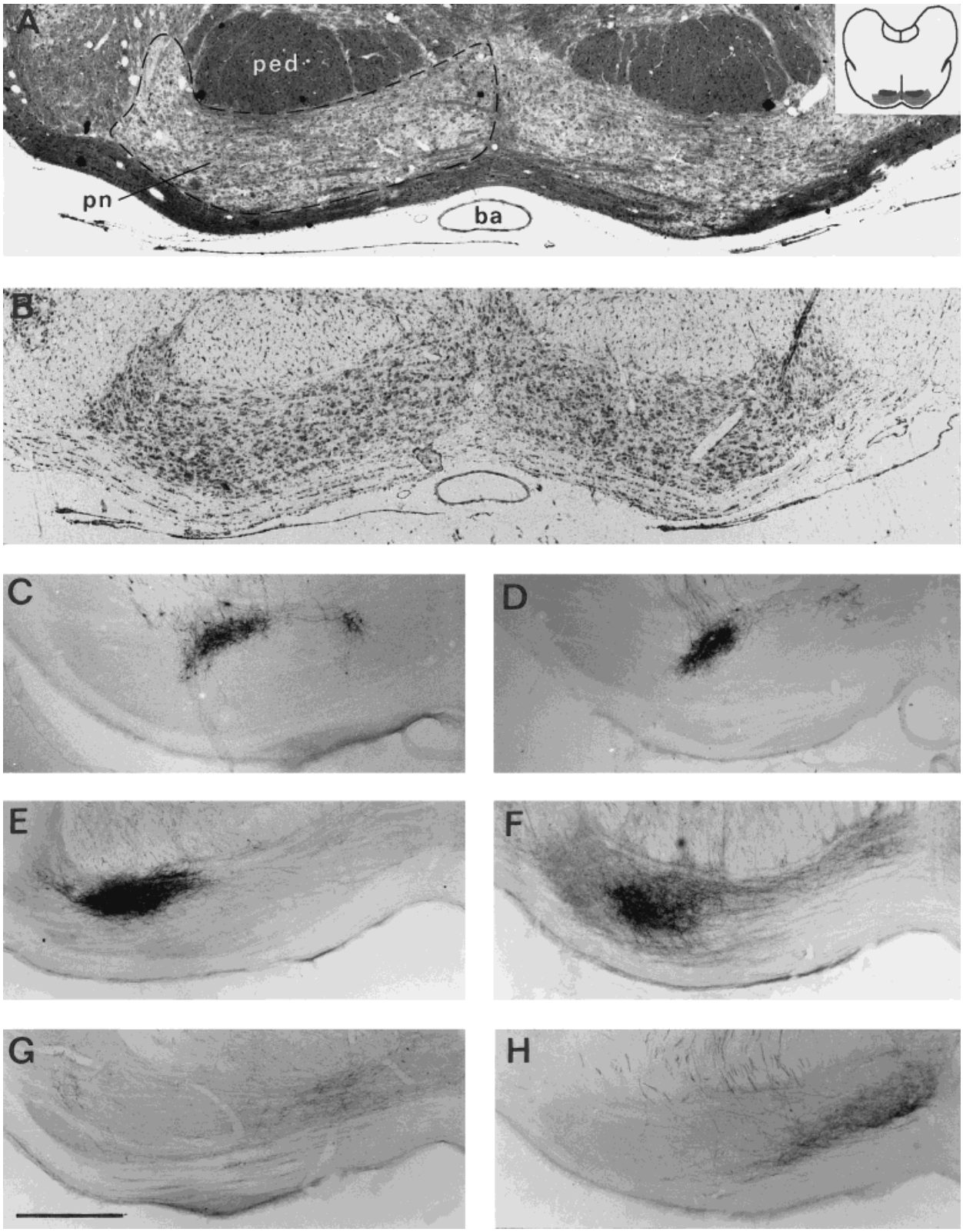

Fig. 3. Photomicrographs of transverse sections through the pontine nuclei in normal material (A,B) and in experimental material (C–H) from animal R106 (C), animal R111 (D), animal R120 (E), animal R124 (F), animal R115 (G), and animal R123 (H; cf. Table 1). The **inset** shows a schematic drawing of a transverse brainstem section corresponding to the photomicrographs. **A,B:** Neighboring sections through the midpontine level stained for myelin and cells (Woelcke and cresyl violet; A) and cells only (thionin; B). The approximate boundary of the right pontine nuclei is indicated by a thin contour line in A. **C,D:** Sections through the right pontine nuclei at the midpontine level showing representative axonal plexuses labeled after injection of *Phaseolus vulgaris*-leucoagglutinin (Pha-l) into the SI upper lip representation. Typically, the upper lip labeling consisted of a large lateral and a small medial axonal plexus, both located dorsally in the pontine nuclei. **E,F:** Sections through the caudal region of the right pontine nuclei showing axonal plexuses labeled after injection of BDA into proximal body representations of SI (E, trunk; F, proximal hindlimb). In both cases, densely labeled plexuses are located dorsolaterally. **G,H:** Sections through the caudal region of the right pontine nuclei showing axonal plexuses labeled after injection of BDA into distal body representations (G, forelimb; H, hindlimb). In both cases, labeled axonal plexuses are located ventromedially. Labeled fibers also are visible more laterally in the pontine nuclei. ba, Basilary artery; ped, peduncle; pn, pontine nuclei. Scale bar = 500 μm.

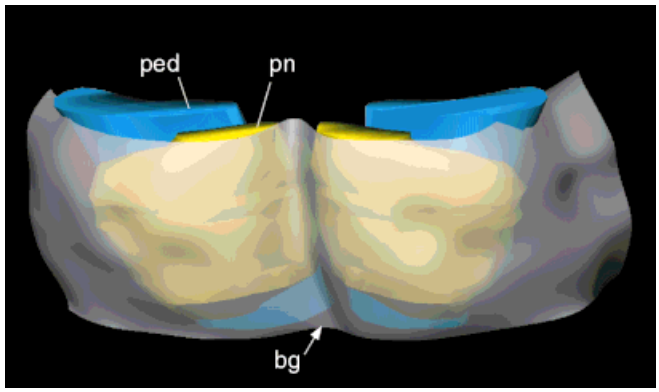

Fig. 4. Computer-generated surface model of the pons in a view from ventral. The external ventral surface of the pons is shown as a transparent gray surface, the pontine nuclei are shown as solid yellow surfaces, and the outlines of the descending fiber tracts (peduncles) are shown as solid blue surfaces. The basilary groove is indicated with an arrow. bg, basilary groove; ped, peduncle; pn, pontine nuclei.

complete axonal trajectory from cortical layer 5 into the ipsilateral pontine nuclei, where the fibers branched extensively to form axonal plexuses (Fig. 3C–F). These *plexuses* of BDA and Pha-l labeling were considered as putative terminal fields.

In addition, we observed beaded varicosities along the trajectories of all of the Pha-l- and BDA-labeled fibers inside the pontine nuclei. It remains to be determined whether these varicosities represent synaptic contacts (Mihailoff et al., 1981). In the corticostriatal projections, however, it has been demonstrated that axonal varicosities contain synaptic vesicles (Kincaid et al., 1998). We have chosen also to include the individual labeled fibers with varicosities in our dot maps.

The labeling was located predominantly in the ipsilateral pontine nuclei, and only sparse labeling was found medially in the contralateral pontine nuclei (Figs. 5, 6). With the Pha-l and BDA labeling, individual fibers could be followed across the midline into the contralateral side. Due to the restricted contralateral labeling, the contralateral pontine nuclei were not mapped further in this study.

3-D cartography of the pontine nuclei

Prompted by the need for precise interindividual comparison, we designed a standard pontine coordinate system for visualizing the distribution of labeling in the pontine nuclei. This allowed us to superimpose the results from different animals. Based on this coordinate system, we made diagrams showing the outlines of the pontine nuclei in ventral, lateral, and rostral views (Fig. 5). In these diagrams, dots were used to show the distribution of labeling, whereas the ventral surface of the pons, the ventral boundary of the descending fiber tract, and the outlines of the pontine nuclei were shown as contour lines (Fig. 5C–E). From each angle of view, a reference frame was introduced that was defined by planes tangential to the rostral, caudal, lateral, and medial boundaries of the pontine nuclei (see also the 3-D visualization of the pontine nuclei in Fig. 4). For spatial reference, we divided the coordinate system into relative values from 0% to 100%, with the intersection of the midline and rostral end of the pontine nuclei as origo. The relative mediolateral or rostrocaudal distance from the origo is given as the percent value. Only the halfway reference lines (50%) are shown in the figures. In the text, we refer to these as the mediolateral 50% line (ml-50 line; *vertical* dashed line in Fig. 5C,E) and the rostrocaudal 50% line (rc-50 line; *horizontal* dashed line in Fig. 5C,D).

The overall distribution of labeling in the pontine nuclei was studied with real-time rotations on the computer screen and was shown to advantage in the complete 3-D reconstructions by using three different angles of view (ventral, medial, and rostral views; Fig. 5). In addition to these standard angles, sections through the reconstructions were useful for demonstrating additional features of the labeling pattern. With the Micro3D software, we prepared series of sections (referred to here as slices) by subdividing the reconstructions at chosen angles and orientations. Figure 6 shows two consecutive series of slices, transverse and sagittal, through one reconstruction. Depending on the plane of slicing, the distribution and shape of the labeling appeared different. In the transverse section plane that is used in most studies of the pontine nuclei (see, e.g., Mihailoff et al., 1978, 1985; Wiesendanger and Wiesendanger, 1982; for reviews, see Brodal and Bjaalie, 1992, 1997), the labeling appeared fairly continuous from rostral to caudal (*columnar*). In contrast, the sagittal series through the same reconstruction revealed two major separated zones of labeling rostrally and caudally in the pontine nuclei. Careful inspection of the reconstructions, therefore, was needed to understand fully the 3-D distribution and shape of the labeling. In addition to showing individual cases in complete reconstructions (Figs. 5, 7–10), we systematically used slices for the further analyses of the distribution patterns and for interindividual comparison (Figs. 11 and 12).

Complete SI projection

To first delineate the extent of the complete SI projection to the pontine nuclei, we attempted to inject as much tracer as possible into SI. In one experiment, a total of 20 injections of BDA were placed throughout SI (Fig. 7A–F). A large, nonuniform area of labeling was found dorsally in the pontine nuclei, relatively close to the descending fiber tract (Fig. 7C,F,I). This was particularly evident in the density gradient analysis (Fig. 7E,F). The highest densities of labeling were found in three regions. Two rounded, high-density regions were located close to the ml-50 line on each side of the rc-50 line, and a third band-like, high-density region was located caudally and medially (Fig. 7D). A sagittal view of the reconstruction revealed the rostrocaudal segregation of the high-density regions (Fig. 7E). In a transverse projection, the regions of highest density formed a dorsally located band relatively close to the descending peduncle (Fig. 7F). In addition to this primary labeling, some labeled fibers also were seen in the rostrolateral part of the pontine nuclei (Fig. 7A, asterisk). Labeling in this region was not observed in any of the cases with single or multiple injections described below and, thus, was assumed to be due to labeling of non-SI projections. In this experiment, to assure the most complete fill of the SI possible, several injections were placed close to the SI border. Also, several of the larger injections encroached on white matter. Therefore, it is likely that some of the labeling in this case originated outside the SI.

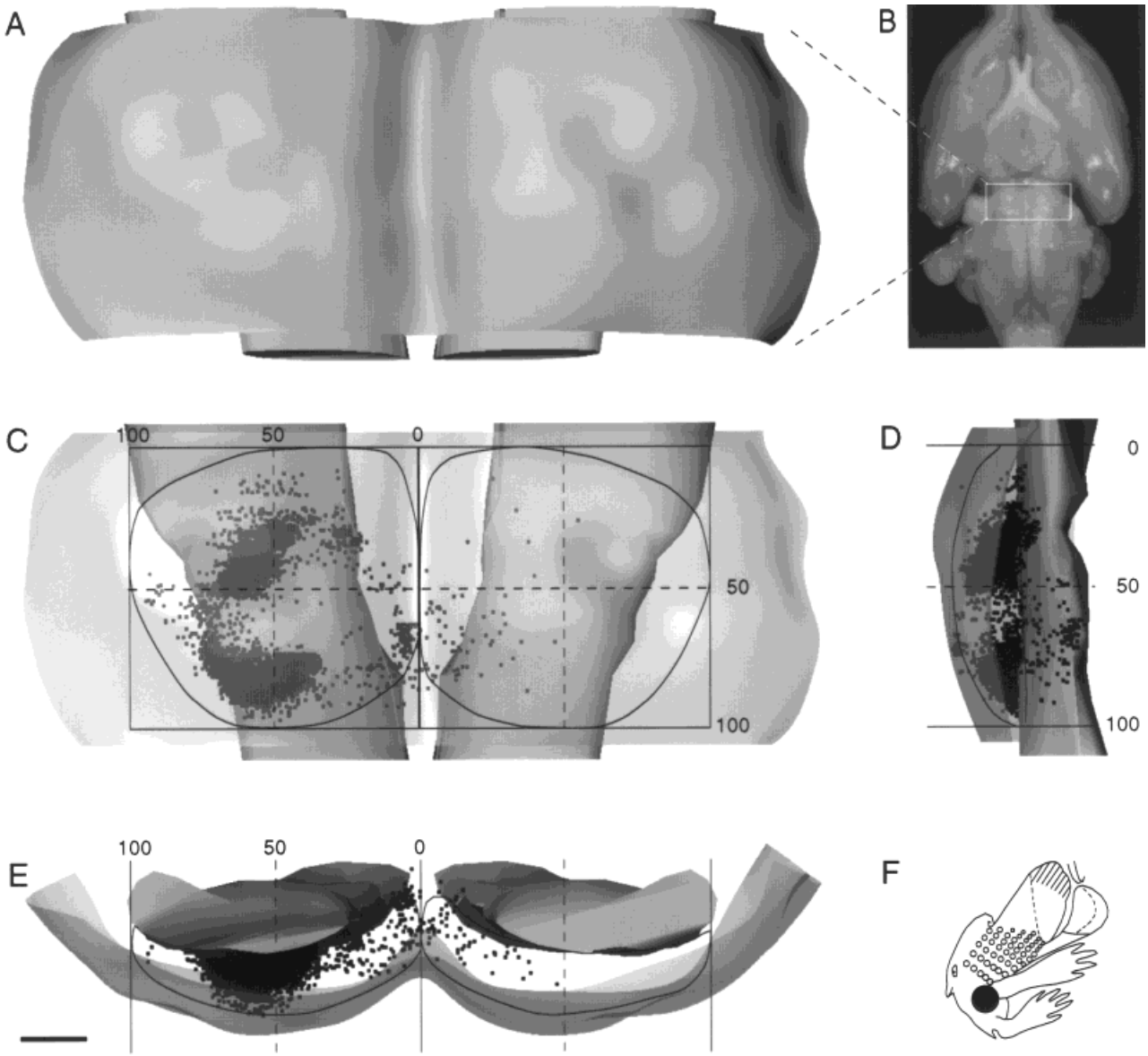

Fig. 5. Computer-generated, three-dimensional (3-D) reconstruction from animal R118, which received an injection of BDA into the trunk representation of SI. **A:** The ventral surface of the pons was resynthesized as a solid surface. The reconstructed descending peduncles are visible as solid surfaces dorsal to the ventral surface in A and in C–E. **B:** Photograph of a rat brain (ventral view). The rectangle indicates the region reconstructed in A, C, D, and E. **C–E:** The ventral surface of the pons is made transparent in C–E. Dots in C–E represent the distribution of BDA-labeled corticopontine fibers within the pontine nuclei. The reconstruction is shown as a total projection right pontine nuclei with an angle of view from ventral (C; perpendicular to the plane of sectioning), medial (D; with the left pons removed), and rostral (E). From each angle of view (C–E), a frame of reference is superimposed onto the model, defined by planes tangential to the boundaries of the pontine nuclei. A coordinate system of relative values from 0% to 100% is introduced. The halfway reference lines (50%) are shown as dashed lines. Curved, continuous lines represent the boundaries of the pontine nuclei. The boundary of the pontine nuclei in D is drawn at the level of the vertical dashed line in C. The boundary of the pontine nuclei in E is drawn at the level of the horizontal dashed line in C. **F:** Standard somatotopic map of the SI showing the size and position of the BDA injection site. Scale bar = 500 μm.

In this experiment, we also observed a zone with low labeling density situated medial to the intersection of ml-50 and rc-50 (Fig. 7A, arrow). This sparsely labeled region was seen consistently in all experiments in this study, regardless of the number of injections made. This phenomenon is not due to inhomogenities in fiber or cellular architecture, as judged from sections stained either with thionin (Fig. 3A) or with combined myelin (Woelcke, 1942) and cresyl violet cell staining (Fig. 3B). Results from other tracing experiments indicate that this region of the pontine nuclei receives afferents from cortical regions anterior and medial to SI (Leergaard and Bjaalie, 1998).

A second, more modest attempt to label a complete projection from SI was made by using ten injections of

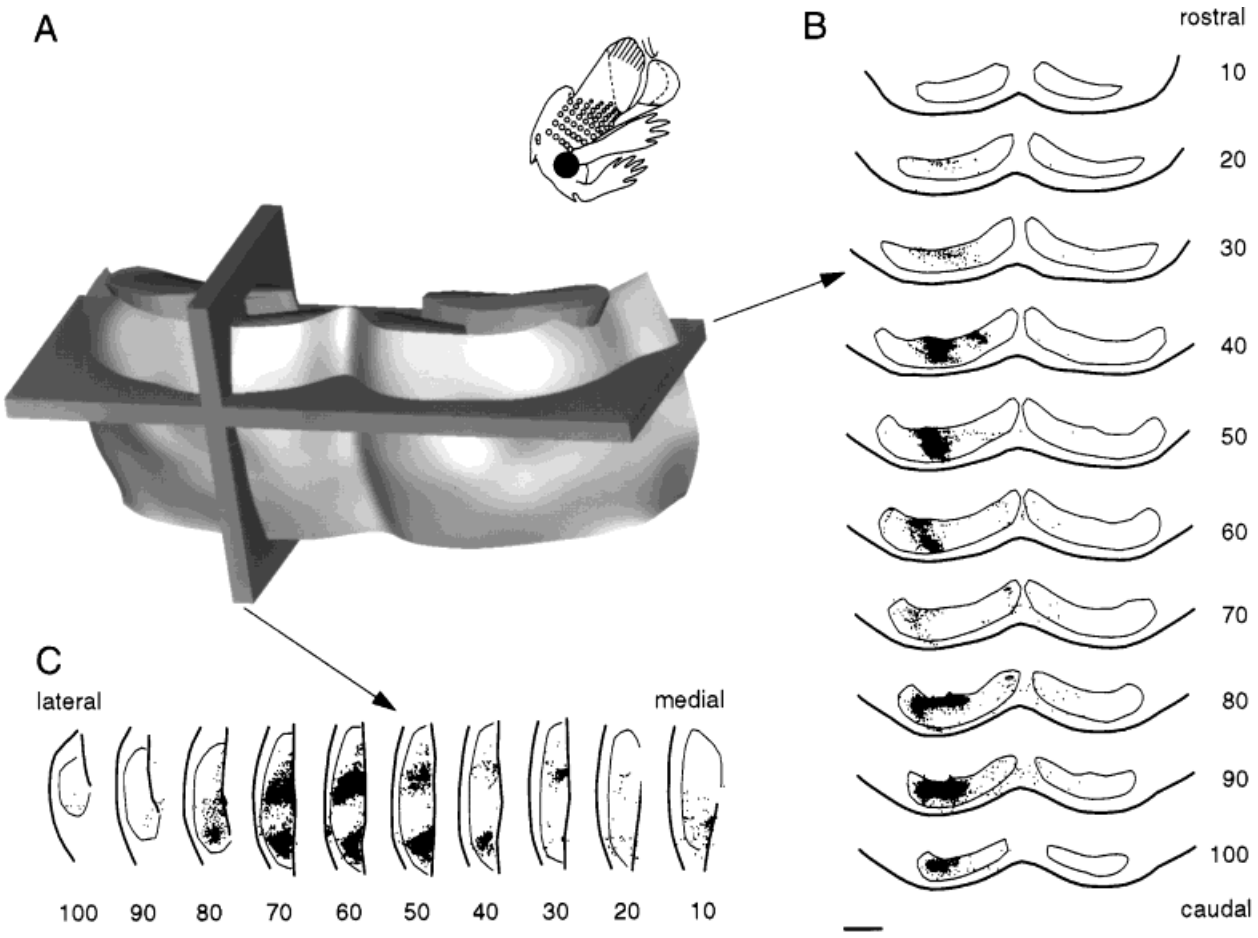

Fig. 6. **A–C:** 3-D reconstruction of the pontine nuclei subdivided into consecutive series of transverse and sagittal slices (BDA injection into the SI trunk representation; the same animal is shown in Fig. 5). The rectangles in A illustrate 200-μm-thick, transverse and sagittal slices shown in B and C, respectively, from the computer reconstruction. The numbers assigned to each slice refer to the coordinate system introduced in Figure 5. Depending on the chosen plane of sectioning, the shapes of the terminal fields appear different. Scale bar = 500 μm.

WGA-HRP (Fig. 7G–I). These injections, however, were positioned to assure at least one injection in each main body representation. In this experiment, care was taken to inject at a distance from the SI border to minimize involvement of adjacent cortical areas, and injection amounts were reduced to minimize the likelihood of white matter labeling. Furthermore, with WGA-HRP, it was expected that the amount of labeling generally would be more limited. The results of this experiment, nevertheless, were very similar to those seen in the case that received 20 injections of BDA into the SI. In both experiments, all labeling was located dorsally, relatively close to the descending fiber tract. In the case that received 10 injections into the SI, two distinct clusters were found centered on the ml-50 line, on each side of the rc-50 line (Fig. 7G). Another solitary cluster was located more rostrally, and two or three clusters were located more caudally. The main differences between these two experiments was the more extensive labeling found rostrally and caudally in the pontine nuclei with the larger number of injection sites.

Thus, from both these experiments, we can conclude that SI corticopontine fibers supply largely the dorsal, central, and caudal regions of the pontine nuclei but that this region is not necessarily labeled uniformly throughout. This projection pattern was explored in more detail by using restricted tracer injections into somatotopically defined subregions of SI.

Projections from SI subregions

Perioral. In one animal, five injections of WGA-HRP were placed in the perioral representation of SI (Fig. 8A–C). The injections covered the representations of the upper lip and the nearest surrounding representations, including the lower lip, the incisors, and the anterolateral barrel subfield. The ensuing labeling in the pontine nuclei was located centrally and was skewed toward the rostral part of the SI projection zone. It consisted of two main clusters, with the largest cluster located mostly lateral to the ml-50 line and predominantly caudal to the rc-50 line. Figure 8A illustrates best that the smaller, medially located cluster was connected to the larger cluster through thin rostral and caudal bridges of fibers. In individual sections, both clusters were located at a distance of approximately 100 μm from the descending fiber tract.

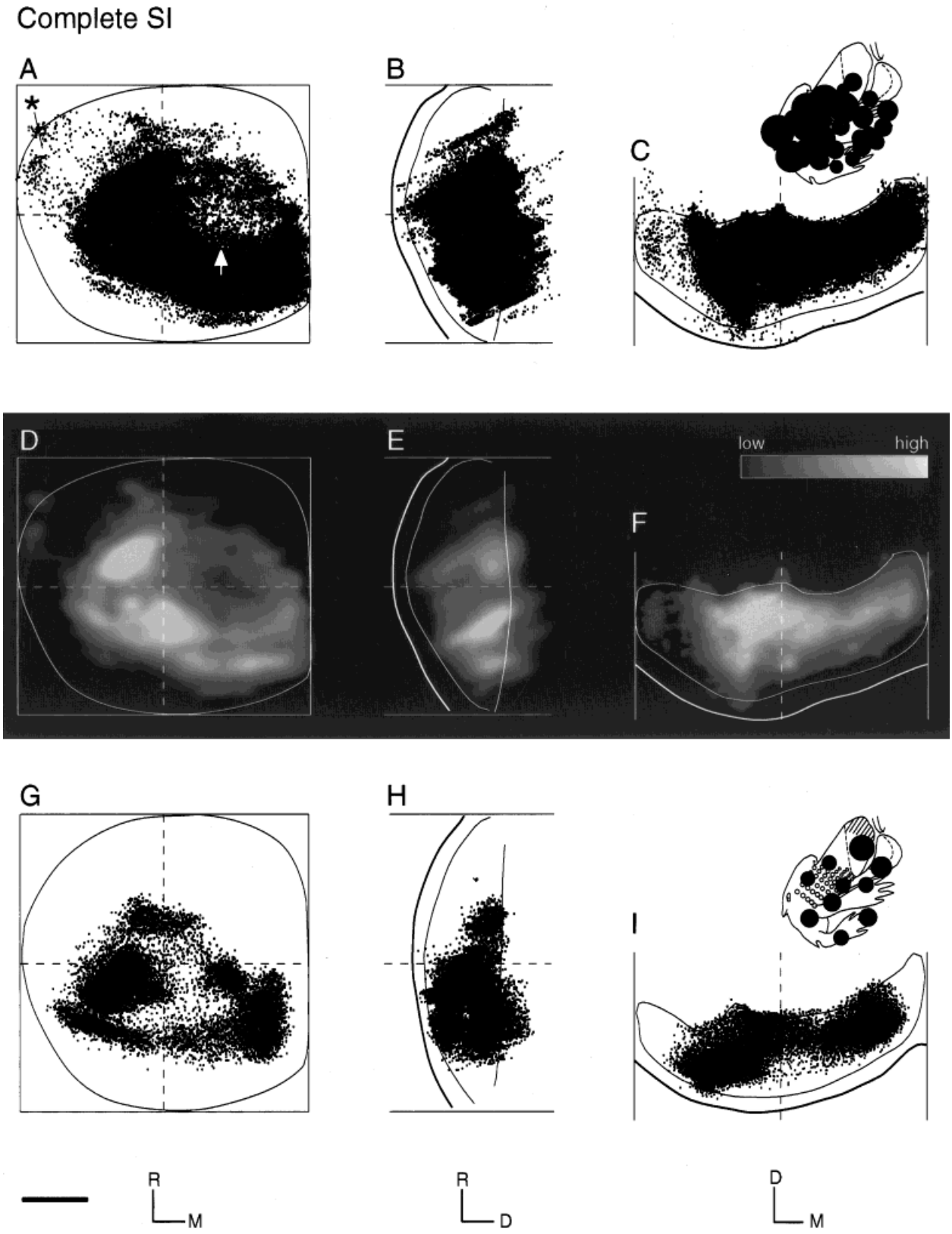

Fig. 7. **A–I:** Computer-generated dot maps (A–C, G–I) and gray scale-coded density maps (D–F) of the distribution of labeling in the right pontine nuclei after multiple injections into SI (A–F, case R102; G–I, case R101; cf. Table 1). The maps are shown as total projections in views from ventral (A,D,G), medial (B,E,H), and rostral (C,F,I) angles (for conventions, see Fig. 5). SI corticopontine fibers supply largely dorsal, central, and caudal regions of the pontine nuclei. The sparse rostrolateral labeling in animal R102 (A, asterisk) may be due to the spread of tracer outside the SI. A zone with a low density of labeling (A, arrow) probably does not receive afferents from SI. D, dorsal; L, lateral; M, medial; R, rostral. Scale bar = 500 μm.

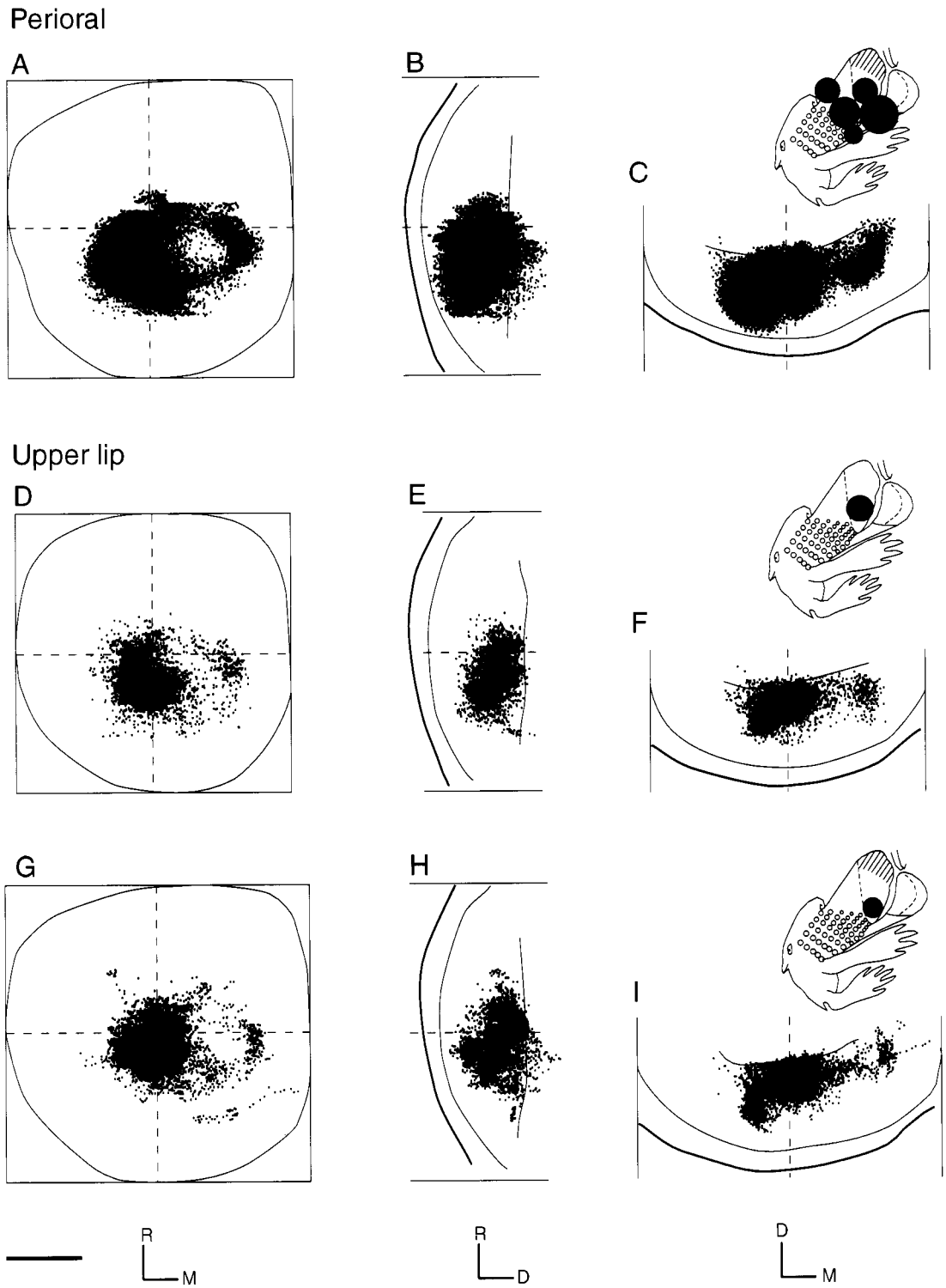

Fig. 8. Computer-generated dot maps (right pontine nuclei, total projections) showing the distribution of pontine labeling after five injections of wheat germ agglutinin-horse radish peroxidase (WGA-HRP) into the perioral representation of SI in case R103 (**A–C**) and single injections of Pha-l in case R106 (**D–F**) and BDA in case R113 (**G–I**) into the upper lip representation of SI (for conventions, see Figs. 5, 7A–C). The distribution of labeling in all three cases is located centrally in the pontine nuclei in a large lateral cluster and a small medial cluster interconnected by more sparsely labeled zones of labeling. The plexuses of pontine upper lip labeling (D–I) are more restricted and fit within the perioral pontine labeling (A–C). Scale bar = 500 μm.

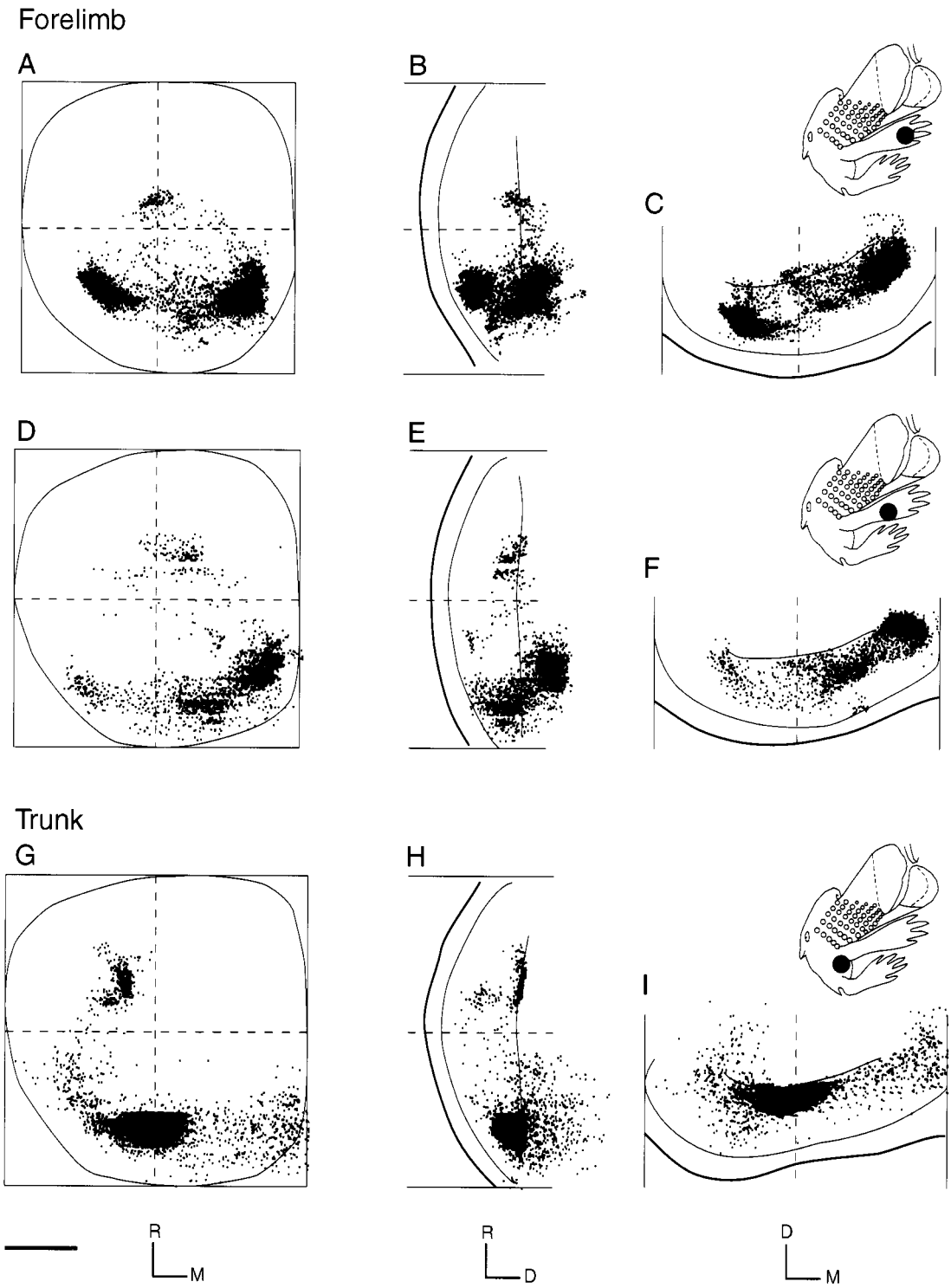

Fig. 9. Computer-generated dot maps (right pontine nuclei, total projections) of the distribution of pontine labeling after injection of BDA into the forelimb representation of SI in case R115 (**A–C**) and case R117 (**D–F**) and into the trunk representation of SI in case R120 (**G–I**; for conventions, see Figs. 5, 7A–C). The labeling in the pontine nuclei consists of two to three clusters adjoining the perioral pontine clusters externally (cf. Fig. 8), typically with a small, centrally located, rostral cluster and a larger, caudal, band-like component, that are widespread in the mediolateral dimension. The proximal trunk representation in the pontine nuclei is shifted laterally compared with the distal forelimb representation (compare D with G). Scale bar = 500 μm.

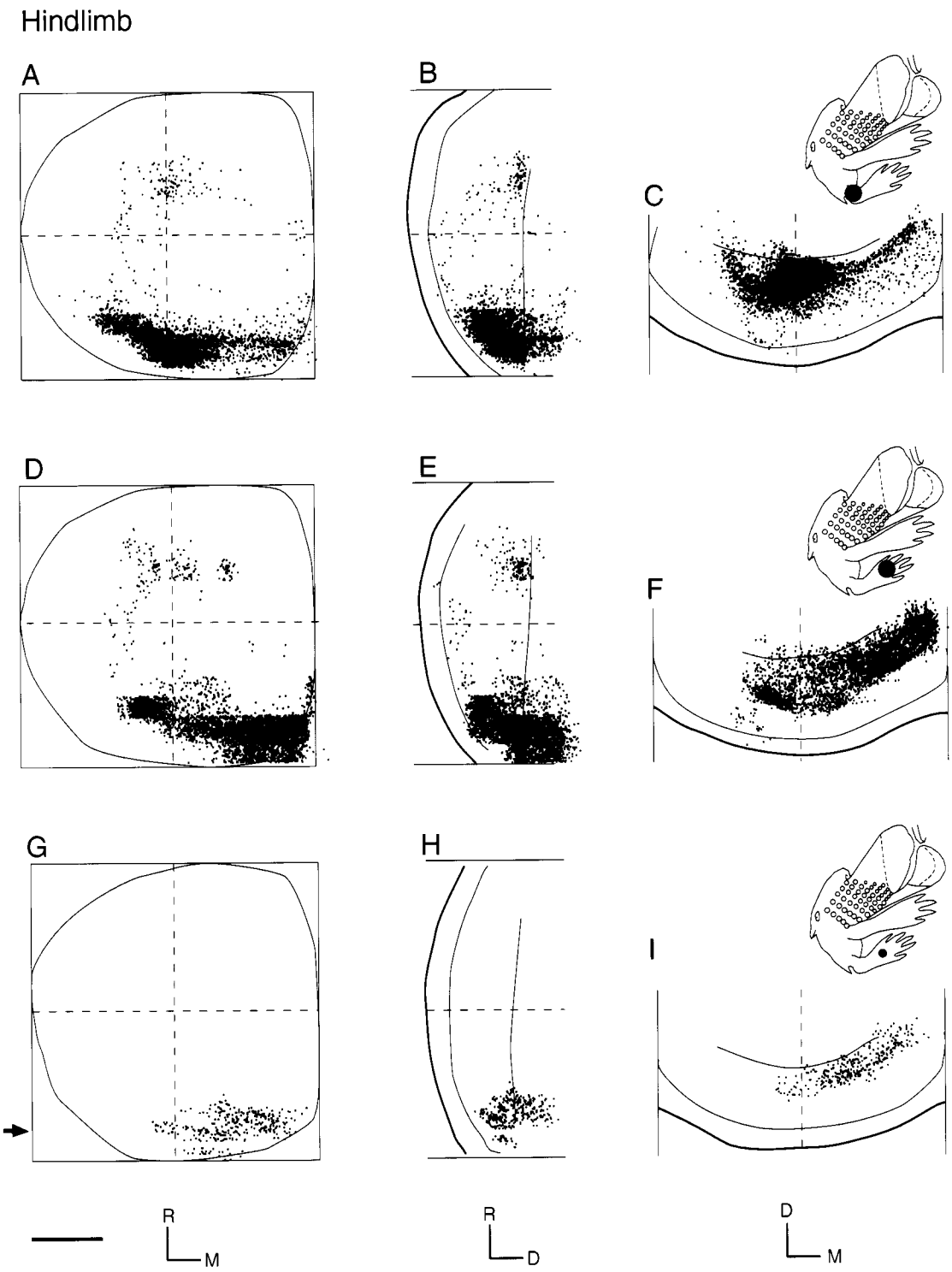

Fig. 10. Computer-generated dot maps (right pontine nuclei, total projections) of the distribution of pontine labeling after injection of BDA into the hindlimb representation of the SI in case R124 (**A–C**), case R123 (**D–F**), and case R125 (**G–I**; for conventions, see Figs. 5, 7A–C). Typically, the labeling is distributed in a caudally located, mediolateral band and in a small, rostral cluster. The proximal hindlimb projection is shifted laterally compared with the distal hindlimb projections (compare A with D and G). The separation between the rostral and caudal components of the pontine labeling is larger than that seen animals that received injections into the SI forelimb representation (cf. Fig. 9). The BDA injection in case R125 (G–I) was very limited, and the pontine labeling was of low density but with a considerable mediolateral extent. The arrow in G indicates the level from which the section in Figure 11 was taken. Scale bar = 500 μm.

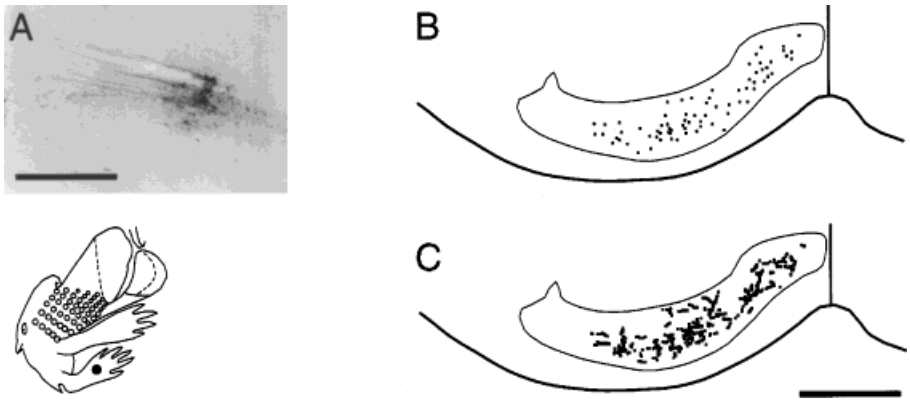

Fig. 11. **A:** Photomicrograph of a limited (200 μm diameter) BDA injection into the SI hindlimb representation (case R125; also illustrated in Fig. 10G–I). **B,C:** Digitized plots of the same single transverse section through the pontine nuclei. The rostrocaudal level of the section is indicated by the arrow in Figure 10G. In B, the labeled axons are plotted semiquantitatively, with point coordinates placed at regular intervals along the length of individual axons. In C, point coordinates were placed side by side along the length of each labeled axon to illustrate the distribution of individual fibers. Scale bar = 500 μm.

Upper lip. Ten rats were injected in the upper lip representation of SI with WGA-HRP, Pha-l, or BDA (Table 1; Fig. 8D–I). Nine cases were computer reconstructed in 3-D. There was only slight variation in the location and extent of labeling among the cases. The upper lip representation projected to a large lateral and a smaller medial cluster (Fig. 8D,G) within the perioral projection area (compare Fig. 8A–C with Fig. 8D–I).

Forelimb. Five rats received injections of BDA into the forelimb representation (Table 1, Fig. 9A–F). The distribution of labeling in the pontine nuclei was consistent among cases, with one cluster of low density located rostral to the rc-50 line and a stronger projection terminating more caudally. The caudal component consisted of a relatively continuous mediolateral band, with two zones of higher density (Fig. 9C,F). Compared with the previously described perioral representation, the forelimb clusters adjoined this projection area externally (Fig. 9A–F, see also Fig. 12E–G).

Trunk. Four animals received injections of BDA into the cortical representation of the trunk and the adjacent proximal forelimb representation (Table 1, Fig. 9G–I, see also Figs. 5, 6). The labeling in these cases generally was located more dorsally and laterally compared with the labeling seen after injections into the distal forelimb representation (Fig. 9, see also Fig. 12). Labeled clusters always were found very close to the peduncle. Also, one of these cases (Figs. 5, 6) contained a much stronger rostral component than any of the other cases mapped in this study. This rostral zone of labeling consisted of two interconnected clusters that were separated in the dorsoventral dimension (Fig. 6B, slice 60). Furthermore, in all cases, smaller clusters of labeling were seen close to the midline.

Hindlimb. Four rats received BDA injections into the hindlimb representation (Table 1, Figs. 10, 11). The labeling was distributed primarily in a band stretching from medial to lateral in the most caudal part of the pontine nuclei and clearly was located more caudally than the forelimb and trunk projections (compare Fig. 9 with Fig. 10). Within this mediolateral band, two to three clusters of higher density were visible (Fig. 10C,F). In all cases but one (Fig. 10G–I), a small rostral cluster was located toward the rostral end of the SI projection area (Fig. 10A,B,D,E). The injection in the proximal hindlimb representation of one animal (Fig. 10A–C) gave rise to a notably stronger lateral labeling compared with the labeling seen in animals that received injections in the distal hindlimb representation (Fig. 10D–I; note that a similar mediolateral difference in the distribution of labeling also is seen when comparing the forelimb and trunk cases; compare Fig. 9 and with Fig. 10).

One of the hindlimb injections (R125; Table 1, Figs. 10G–I, 11) was smaller than the other injections. The injection site (≈200 μm diameter) contained about 100 labeled pyramidal neurons in layer V (estimate of total number of labeled cell bodies from counts in serial sections). The extent of the labeling was narrower than in the other three hindlimb cases but was widespread compared with the small size of the injection site. The labeled fibers formed a loose plexus caudally in the pontine nuclei. No rostral labeling was found in this case. The most marked difference between this case and the other cases with larger injections in the hindlimb region was the very low density of labeling.

Pontine 3-D somatotopic map

To determine the overall mapping of major SI body representations onto the pontine nuclei, we transferred data from 14 of 22 reconstructed cases into the standard pontine coordinate system (see above). These data were fully representative for all body representations investigated. Different features of the ensuing topography are illustrated in selected combinations of cases and in selected transverse and sagittal slices through these cases (Fig. 12). We consider that the accumulated data, as presented in Figure 12, is realistic for the SI mapping onto the pontine nuclei for two major reasons: 1) We have shown that there is a consistent projection pattern for each SI body representation onto the pontine nuclei. For example, with as many as ten cases injected in the electrophysiologically defined upper lip representation, the variation among cases is no larger than the variation between the two upper lip cases shown in Figure 8. This makes our data suitable for interindividual comparison.

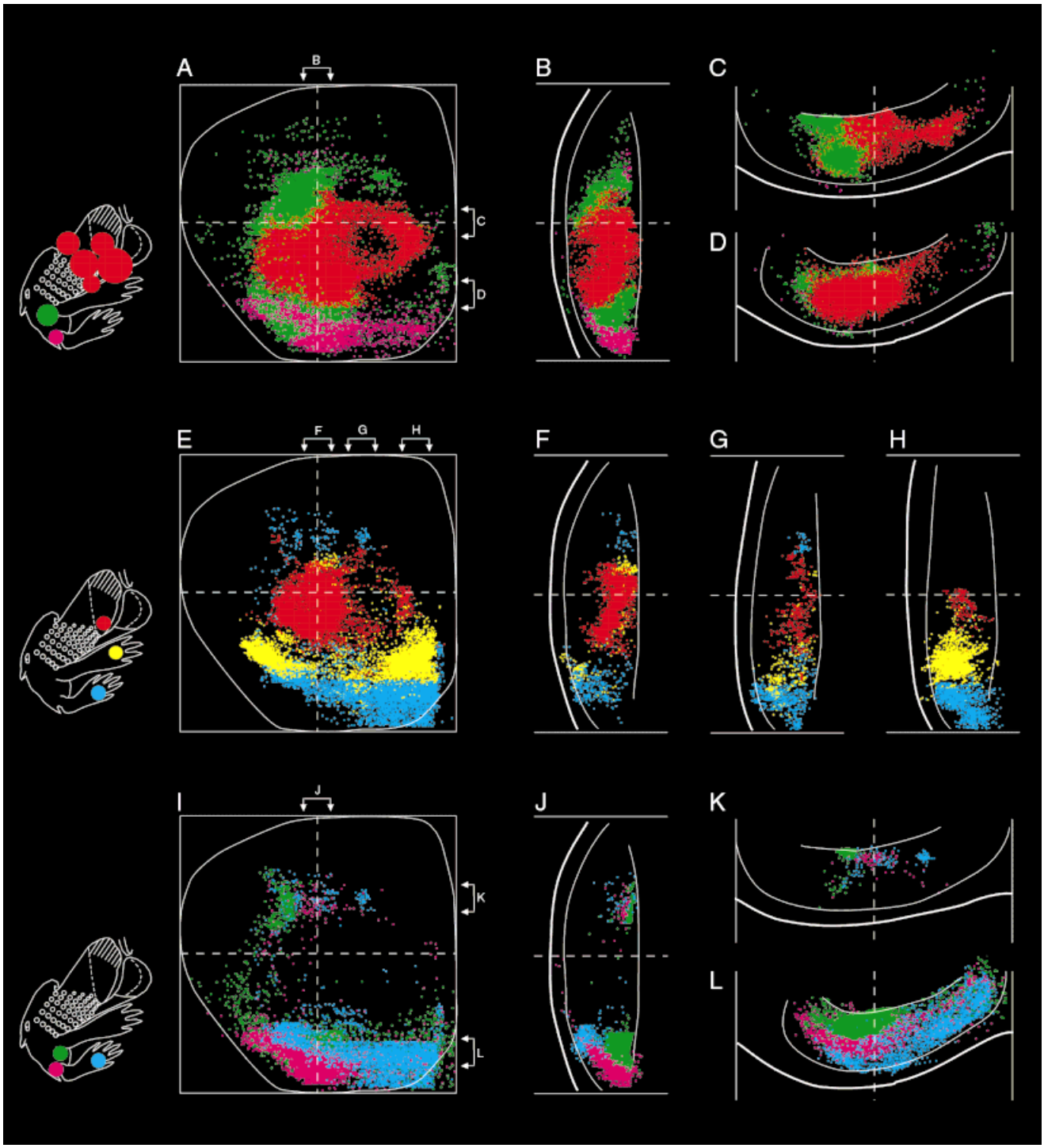

Fig. 12. Computer-generated dot maps (right pontine nuclei; A, E, and C are total projections, and the other images are from 200-μm-thick sections) of the distribution of pontine labeling after tracer injections into various parts of SI. Data from seven individual cases were superimposed in one reconstruction. The spatial relation among different body representations is illustrated by three different combinations of cases. **A–D:** Dot maps showing the perioral representation (red dots, case R103), the trunk representation (green dots, case R118), and the proximal hindlimb representation (pink dots, case R124). **E–H:** Dot maps showing the upper lip representation (red dots, case 113), the distal forelimb representation (yellow dots, case R115) and the distal hindlimb representation (blue dots, case R123). **I–L:** Dot maps showing the trunk representation (green dots, case 120), the proximal hindlimb representation (pink dots, case R124), and the distal hindlimb repesentation (blue dots, case R123). A, E, and I show ventral views. The location of selected 200-μm-thick sagittal slices (B,F–H,J), and transverse slices (C–D,K–L) are indicated by paired arrows in A, E, and I (for conventions see Figs. 5, 7A–C). Shifts of cortical site of origin correspond to systemic shifts of distribution of pontine labeling.

2) We have taken several precautions when transferring reconstructions from different animals into the standard pontine coordinate system. First, each reconstruction was scaled to an average size (2 mm × 2 mm for the frame boundaries in the ventral view; cf. Fig. 6) to rule out the linear variation (≈ 10%) in the rostrocaudal and mediolateral dimensions of the pontine nuclei. Second, multiple reference lines (ventral surface, peduncle, midline, and other; see Materials and Methods) were used as a basis for superimposing data.

To elucidate general organizing principles of the SI-pontine projection, the mapping of different SI body representations is outlined below in three examples, with each example combining three body representations. In the first example, we compared the mapping of the *perioral*, *trunk*, and *proximal hindlimb* representations (Fig. 12A–D). In the cerebral cortex, this sequence of body representations corresponds to a shift from lateral (perioral) to medial. In the pontine nuclei, the perioral representation projected to an internal region (Fig. 12A–D, red dots), whereas the trunk and proximal hindlimb representations projected to progressively more external regions (Fig. 12A–D, green and pink dots, respectively). The projection from the trunk representation (Fig. 12A–D, green dots) partly surrounded the perioral projection laterally and dorsally in the pontine nuclei. This was particularly evident in the sagittal and transverse clip planes through the rostral end of the reconstruction (Fig. 12B–D). The proximal hindlimb projection (Fig. 12A–D, purple dots), which originates farther medial in SI, curved around the trunk representations in a more caudal (and thus more externally located) subspace. A similar internal-to-external shift in the pontine nuclei also is shown in Figure 12J,L [compare green dots (trunk) with purple dots (proximal hindlimb)].

In the second example, the mapping of the *upper lip*, *forelimb*, and *hindlimb* representations were compared (Fig. 12E–H). In the cerebral cortex, this sequence again corresponds to a shift from lateral (upper lip) toward medial and, in the pontine nuclei of our material, from internal to external. The external component (Fig. 12E–H, yellow and blue dots) was located primarily in the caudal part of the pontine nuclei. There was only a very small projection from the limb representations rostral to the upper lip projection (see also Figs. 9, 10). The rostral forelimb projection, on average, was closer to the rc-50 line than the rostral hindlimb projection. The topographic specificity in this rostral part, however, was less apparent than in the caudal part. The upper lip was located inside the perioral projection [compare Fig. 12E, red dots (upper lip) with Fig. 12A, red dots (perioral)], whereas the limb projections formed clusters or horizontal bands in progressively more caudal parts of the pontine nuclei.

In the third example, we compared the projections from the *trunk*, *proximal hindlimb*, and *distal hindlimb* representations (Fig. 12I–L). Trunk and proximal body parts were represented more posteriorly in SI than the distal limbs. A shift in SI site of origin from posterior to anterior (from proximal to distal body representations) corresponded to an overall shift from lateral to medial in the pontine nuclei (Fig. 12I–L). However, as pointed out above, several of these projections tended to spread out horizontally. The main difference, therefore, was the lateral or medial predominance of labeling (Fig. 12I,L; note the lateral predominance of purple dots corresponding to the proximal hindlimb and the medial predominance of blue dots corresponding to the distal hindlimb). A mediolateral difference in distribution of labeling also is seen in Figure 12A,E (limb projections, shown as yellow and blue dots in Fig. 12E, were skewed more toward medial than proximal body projections, which are shown as green and purple dots in Fig. 12A).

In a final analysis, we employed computer-generated surfaces to demonstrate the outer boundaries of the clusters of labeling from the different body representations (Fig. 13). Data from 14 representative cases served as the basis for this model. The surfaces also surround regions of intermediate and lower labeling density, thereby emphasizing the continuity of labeling. Regions with the lowest densities at the periphery of the main clusters were excluded (for further details, see Materials and Methods). This approach shows to advantage the 3-D location and shape of the pontine regions receiving projections from a given SI body representation. The zones of labeling formed different shapes, ranging from 3-D spheroids to cylindroids (in 2-D; circle-like and band-like shapes). Adjacent spheroids and cylindroids were complementary in shape and, together, formed a 3-D mosaic, with each major body representation represented in its own territory. The perioral region mapped in the current study (and the remaining part of the face area; T.B. Leergaard, K.D. Alloway, J.J. Mutic, and J.G. Bjaalie, unpublished observations of the corticopontine projection from individual whisker barrels) occupied mainly the internal and central part of the pontine nuclei (Fig. 13B, red). The other body parts were represented in multiple locations surrounding the face, primarily caudally, but also in smaller rostral subdivisions. Figure 12 also shows that the neighboring relationships in the SI somatotopic map (Fig. 13A) largely were preserved in the pontine map (Fig. 13B,C).

In summary, we have shown that a given linear shift in location of SI site of origin, gives rise to a systematic shift in location of pontine terminal fields of labeling. We have outlined two such shifts: 1) a shift from *lateral to medial in SI* (i.e., from perioral to forelimb and hindlimb representations or from perioral to trunk and proximal hindlimb representations) corresponded to an *internal-to-external shift in location of pontine terminal fields*. This overall internal-to-external mapping in the pontine nuclei is in agreement with developmental data (Fig. 14; Leergaard et al., 1995). In young rats, a 3-D, lamellar organization is seen (Leergaard et al., 1995). The clusters of labeling observed in the current study of adult animals were distributed following the same principles that were observed in young animals (see Discussion) and, thus, may be interpreted as parts of lamellar subspaces or shells that are organized in an inside-out fashion (compare sagittal slices in Fig. 12 with developmental hypothesis in Fig. 14). 2) A shift from *anterior to posterior in SI* (i.e., from distal body parts to proximal body parts) corresponded to a *medial-to-lateral shift in location of pontine terminal fields*. Each body representation in the SI generally gave rise to terminal fields that were widespread from medial to lateral, but the densities of the projections varied from medial to lateral. This overall medial-to-lateral mapping in the pontine nuclei corresponds well with previously described topographic principles (Mihailoff et al., 1978; Wiesendanger and Wiesendanger, 1982; additional original data can be viewed at http://www.nesys.uio.no/ and http://www.cerebellum.org/).

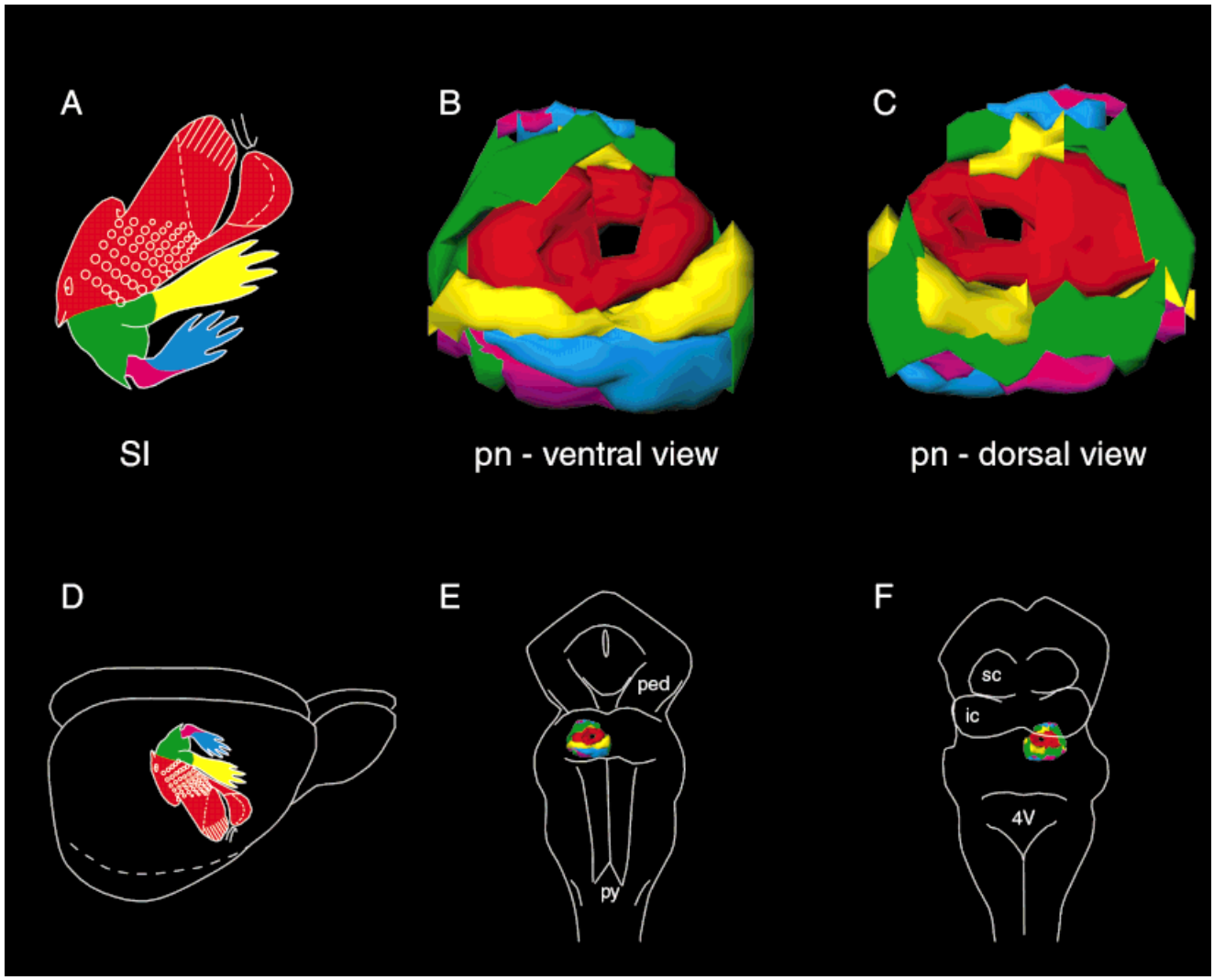

Fig. 13. 3-D surface model of the projections from individual SI body representations to the pontine nuclei. The basis for this model was a reconstruction of the same type shown in Figure 12 but with data from a larger number of animals included. The reconstruction was divided into a series of sagittal slices, and these slices were used as a basis for defining contour lines surrounding the zones of labeling. The main body representations in the SI body map are color coded (**A**; the same colors are used in Fig. 12), and the same colors are used for showing the distribution of the corresponding clustered pontine projection regions (**B,C**). The angle of orientation of the SI somatotopic map in A is chosen to facilitate comparison with the pontine somatotopic map in the ventral view (B). The line drawing in **D** indicates the position of the SI body map in the right cerebral hemisphere. Line drawings of the brainstem (**E,F**) indicate the position of the SI pontine projection regions modeled in B and C, respectively. In B and C, the concentric arrangement of the clusters from internal to external is apparent. Thus, a particular SI body representation projects to several clusters in the pontine nuclei. Nevertheless, the spatial relationships in the cerebral cortical map largely are preserved in the 3-D, clustered pontine map. 4V, fourth ventricle; ic, inferior colliculus; ped, peduncle; pn, pontine nuclei; py, pyramidal decussation; sc, superior colliculus.

DISCUSSION

By the combined use of electrophysiologically guided tract tracing and 3-D computerized reconstructions, we have mapped the somatotopically organized projection from SI to the pontine nuclei. In SI, there is an essentially continuous body representation (Welker, 1971, 1976; Chapin and Lin, 1984; for review, see Chapin and Lin, 1990). In the pontine nuclei, this map is transformed to a more complex pattern that is characterized by 1) multiple, separate terminal fields for each body representation; 2) an internal-to-external, shell-like organization with perioral representations internally and extremity and trunk representations more externally; and 3) largely maintained spatial relationships among the pontine projections from the major SI body representations. Consequently, the pontine nuclei appear to contain several representations of the SI map, with each largely preserving the general spatial relationships of the SI map.

Due to the difficulties inherent to the analysis of noncortical structures, the use of computerized, 3-D reconstruction and visualization techniques was essential for the mapping of the complex SI-pontine projection. To assure accuracy and consistency across experiments, it was critical to define the injection sites physiologically. Fur-

thermore, to understand the overall pattern of SI projections, it was necessary to perform a series of injections of different sizes in different regions of the SI map. This, in turn, made it necessary to develop a standard representation of the pontine nuclei so that the results from injections into different animals (Fig. 12) could be compared quantitatively. The results revealed that the projection pattern for each SI body representation was highly reproducible between animals.

Establishment of topographic patterns

The internal-to-external, shell-like organization of the pontine nuclei reported in this study is interesting in the context of the establishment of subcortical projections in general. In the cerebral cortex, anterior and lateral parts are established before more medial and posterior parts (Hicks and D'Amato, 1968; Smart, 1984; see also Miller, 1987; Erzurumlu and Jhaveri, 1992). Thus, a shift in the cortical site of origin from lateral to medial (in SI, from perioral representations to hindlimb representations) follows the cortical neurogenetic gradient. Indeed, within SI, electrophysiological specificity develops from lateral to medial (McCandlish et al., 1993). Similarly, the internal region of the pontine nuclei is established before more external parts (Altman and Bayer, 1978, 1987). Thus, the internal-to-external shift in the distribution of SI afferents in the pontine nuclei (Figs. 12, 13) would appear to follow the temporal settling of pontine neurons. The present data, therefore, support the view that, in developmental terms, there are temporal and spatial relationships between cortical site of origin and pontine target region. A hypothesis explaining the establishment of corticopontine topography, which was presented in Leergaard et al. (1995), is shown in Figure 14.

Shape of terminal fields

The current data shed further light on basic anatomic principles of organization in the pontine nuclei. Major cortical regions (visual, somatosensory, motor, and other) have a patchy (clustered in 3-D) and divergent topography but, nevertheless, are mapped onto the pontine nuclei in an orderly fashion (for reviews, see Brodal and Bjaalie, 1992, 1997). Most of the early studies of the corticopontine projection in the cat (Brodal, 1968) and rat (Mihailoff et al., 1978, 1984, 1985; Wiesendanger and Wiesendanger, 1982; Lee and Mihailoff, 1990; Panto et al., 1995) emphasized a rostrocaudal columnar organization of the somatosensory and other corticopontine projection fields. This is not surprising, because, in transverse sections (used by most investigators), the tendency for a rostrocaudal continuity of terminal fields is seen readily (see also our transverse slices, which are exemplified in Fig. 6). In the current study, however, by using 3-D, computerized analyses of complete series of sections, we have demonstrated that the terminal fields of somatosensory corticopontine

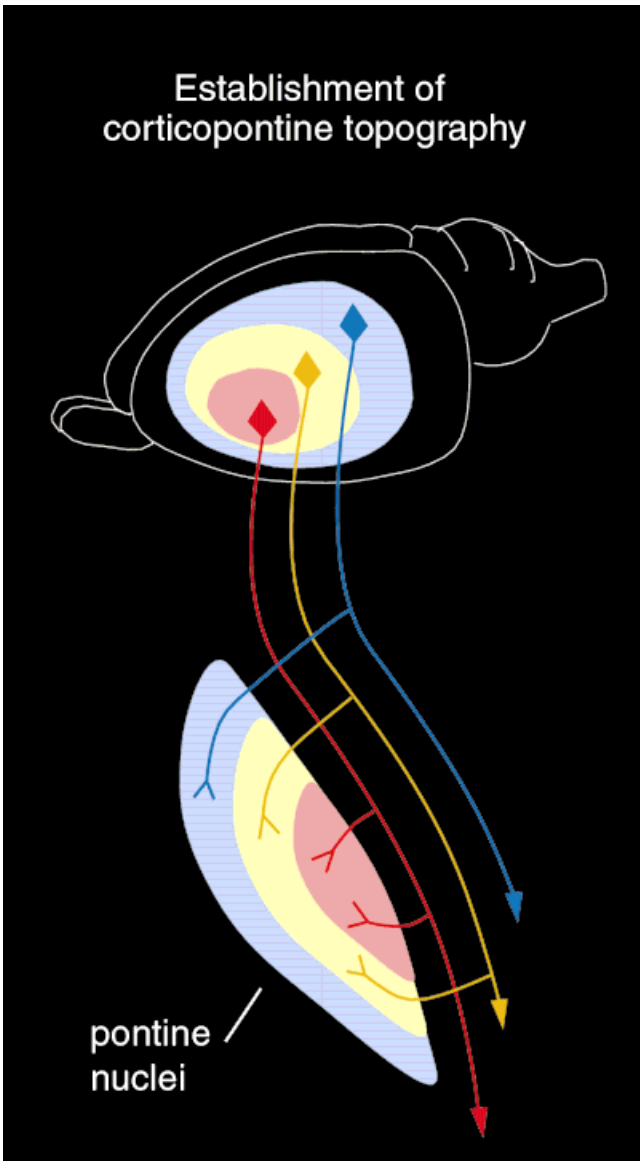

Fig. 14. Cartoon of the hypothesis explaining the establishment of general topographic organization in the rat corticopontine system (Leergaard et al., 1995). The cerebral neurogenetic gradient ripples outward from the anterolateral cortex (Hicks and D'Amato, 1968; Smart, 1984), and the cerebral axonogenetic gradient is presumed to follow the neurogenetic gradient (Gribnau et al., 1986; O'Leary and Terashima, 1988; DeCarlos and O'Leary, 1992; Erzurumlu and Jhaveri, 1992). Altman and Bayer (1978, 1987) reported that neurons in the pontine nuclei settled inside-out in a pattern of concentric rings (presumable layers in 3-D) in a temporal sequence. Corticopontine fibers grow into the pontine nuclei around the time of birth (O'Leary and Terashima, 1988), attracted by chemotropic cues that are produced by neurons in the pontine nuclei (Heffner et al., 1990; O'Leary et al., 1991; Bastmeyer et al., 1998). In a recent study of young rats (newborn and up to postnatal day 7; Leergaard et al., 1995), we showed that corticopontine axons originating in different locations of the cortex occupied lamella-shaped zones in the pontine nuclei and that there were systematic shifts of pontine projection regions corresponding to linear shifts of the cortical site of origin. The temporal gradients, from early to later, are illustrated by the colors red, yellow, and blue. Early arriving corticopontine fibers innervate the early established central core of the pontine nuclei (red), whereas later arriving fibers innervate progressively more external volumes (yellow and blue). The topographic mapping of the SI cortex onto the pontine nuclei reported in the current paper is compatible with this distribution gradient. Several cortical efferent systems (corticostriatal: Bayer and Altman, 1987; corticothalamic: Bolz et al., 1990, 1993; Novak and Bolz, 1993; corticospinal: Joosten et al., 1991, 1993, 1994) and afferent systems (thalamocortical: Götz et al., 1992; Bolz et al., 1992) display characteristics suggestive of similar developmental principles.

axons are not distributed primarily in rostrocaudal columns but, rather, in curved and elongated clusters with a mediolateral orientation. We interpret the complementary shape and systematic shifts (inside-out arrangement) of these clusters as reminiscent of a "shell-like" or "lamellar" organization, which was demonstrated previously in the newborn rat (Leergaard et al., 1995). Lamellae of corticopontine terminal fields for other corticopontine projections have been reported in the adult monkey (Brodal, 1978) and the adult cat (Bjaalie et al., 1997b; see also Aas and Brodal, 1989; Bjaalie and Brodal, 1989; Brodal et al., 1991). Our study provides the first evidence in the adult rat for a pattern that is reminiscent of the lamellar organization demonstrated previously in the newborn rat (Leergaard et al., 1995).

Pontine somatotopic mapping: Anatomy to function

The current results allow for the first time a direct comparison of the complex, 3-D pontine map with the essentially 2-D cortical map for the same sensory modality. The pontine somatotopic map differs from that in SI in several respects. For a particular body representation, the 3-D pattern of multiple, elongated clusters in the pontine nuclei appears to create an increased interface between neighboring body representations. For example, in SI, the proximal hindlimb representation occupies a small area with a *restricted* interface toward adjacent body representations (trunk and distal hindlimb). In the pontine nuclei, however, the proximal hindlimb is represented primarily in an elongated cluster. This cluster has a large interface with similarly elongated clusters for neighboring body representations (note the neighboring relationships of pink dots in Fig. 12A,B,I,J,L; see also Fig. 13B,C). Furthermore, the widespread clusters in the pontine nuclei also seem to form *neighboring relationships* that are not evident in the SI body map. For example, as shown in Figure 12B, the proximal hindlimb representation (Fig. 12B, pink dots) curves around the trunk representation (Fig. 12B, green dots) and encroaches upon the perioral representation (Fig. 12B, red dots). Another example is found in the rostral region of the pontine somatosensory map, in which upper lip, forelimb, and hindlimb clusters are in close proximity (Fig. 12F,G; see also Fig. 13B,C). In this way, the topographic organization of the pontine nuclei may foreshadow the much more extensive intermixing of representations of tactile surfaces seen in the highly fractured maps of the cerebellum (Bower and Kassel, 1990).

Close spatial relationships among pontine terminal fields of axons that originate in different parts of the cerebral cortex may represent in part the substrate for large receptive fields of pontine neurons (Rüegg and Wiesendanger, 1975; Rüegg et al., 1977; Potter et al., 1978; see also Baker et al., 1976; Thier et al., 1988; Suzuki et al., 1990; Mihailoff et al., 1992). The degree of functional overlap among different terminal fields and convergence of input onto single pontine neurons, however, is highly dependent on the extent of dendritic arbors of pontine neurons. Schwarz and Thier (1995) emphasized a compartmental organization with dendritic trees of pontocerebellar neurons largely respecting individual terminal fields of corticopontine axons. In contrast, Mihailoff et al. (1981) found pontine neurons with dendrites probably extending into more than one afferent projection area. Also, as demonstrated in several single- and double-anterograde tracing studies, there is a certain degree of overlap of terminal fields from adjacent cortical locations (Mihailoff et al., 1985; Schwartz and Thier, 1995). After the injection of two different tracers into individual SI whisker barrels, predictable shifts and partially overlapping projection fields were seen (T.B. Leergaard, K.D. Alloway, J.J. Mutic, and J.G. Bjaalie, unpublished observations).

The orderly mapping, combined with the widespread distribution of the pontine terminal fields, thus, may serve to integrate somatosensory signals from adjacent body representations and to combine these with information of a different modality from other regions of the cerebral cortex and from subcortical sources of afferents to the pontine nuclei. Specific convergences in the pontine nuclei among projections from different cortical sites and among cortical and subcortical projections have been described (Mihailoff et al., 1985, 1989; Kosinski et al., 1986, 1988; Aas and Brodal, 1989; Bjaalie and Brodal, 1989; Lee and Mihailoff, 1990; Mihailoff, 1995; see also Mihailoff et al., 1992).

Transformations from continuous to fractured maps

The recent proposal by Bower (for review, see Bower, 1997) that the hemispheres of the cerebellum may be involved primarily in the control of somatosensory data acquisition rests substantially on the unusual, fractured pattern of tactile projections to these regions (for references, see Bower and Kassel, 1990). In addition, this theory implies an important modulatory role for the information arising in SI and projecting to these same cerebellar regions. Furthermore, a recent examinations of cerebellar map plasticity (Gonzales et al., 1993; Shumway et al., 1999) after both neonatal and adult peripheral lesions suggest that all cerebellar map plasticity is an indirect consequence of the reorganization in afferent structures (like the trigeminal nucleus and SI). For these reasons, it is critical to understand better the contribution of the pontine nuclei to the topographic transformation from SI mapping to cerebellar mapping.

From the current finding that the spatial relationships of the SI continuous body representations largely are preserved in the pontine nuclei, it is unlikely that the discontinuous nature of the cerebellar fractured maps is present already in the SI-pontine projection. Studies of cerebellar afferents show that pontocerebellar mossy fibers are highly collateralized (for references, see Bjaalie and Brodal, 1997). This axonal branching may be associated with the fractured pattern of cerebellar mapping. Consistent with this interpretation, physiological data suggest that axonal collateralization underlies the fractured projection of the mossy fiber trigeminocerebellar pathway (Woolston et al., 1981).

The fractured cerebellar mapping is characterized not only by topographic discontinuity but also by multiple representations of the body surface in the cerebellum. It is not known whether the multiple, clustered body representations in the pontine nuclei contribute to this feature of the cerebellar maps. However, the results reported in this paper now lay the groundwork for a quantitative, physiologically defined investigation of the projection pattern from the pontine nuclei to the cerebellum. With the completion of that study, we ex-

pect to understand for the first time the anatomic patterns underlying the influence of SI on the cerebellar hemispheres.

ACKNOWLEDGMENTS

Financial support was provided by European Community grant Bio4 CT98-0182, The Research Council of Norway, and National Institutes of Health grant NS37109. The authors thank Drs. Per Brodal and Kirsten Osen for valuable comments and E.O. Andersen, A.T. Bore, C. Knudsen, G.F. Lothe, and C. Pettersen for expert technical assistance. T.B.L. and K.A.L. contributed equally to this paper.

LITERATURE CITED

Aas J-E, Brodal P. 1989. Demonstration of a mamillo-ponto-cerebellar pathway. A multi-tracer study. Eur J Neurosci 1:61–74.

Altman J, Bayer SA. 1978. Prenatal development of the cerebellar system in the rat. II. Cytogenesis and histogenesis of the inferior olive, pontine gray, and the precerebellar reticular nuclei. J Comp Neurol 179:49–75.

Altman J, Bayer SA. 1987. Development of the precerebellar nuclei in the rat. IV. The anterior precerebellar extramural migratory stream and the nucleus reticularis tegmenti pontis and the basal pontine gray. J Comp Neurol 257:529–552.

Bajo VM, Merchan MA, Malmierca MS, Nodal FR, Bjaalie JG. 1999. Topographic organization of the dorsal nucleus of the lateral lemniscus in the cat. J Comp Neurol 407:349–366.

Baker J, Gibson A, Glickstein M, Stein J. 1976. Visual cells in the pontine nuclei of the cat. J Physiol (London) 255:415–433.

Bastmeyer M, Daston MM, Possel H, O'Leary DD. 1998. Collateral branch formation related to cellular structures in the axon tract during corticopontine target recognition. J Comp Neurol 392:1–18.

Bayer SA, Altman J. 1987. Directions in neurogenetic gradients and patterns of anatomical connections in the telencephalon. Progr Neurobiol 29:57–106.

Berg BG, Almaas TJ, Bjaalie JG, Mustaparta H. 1998. The macroglomerular complex of the antennal lobe in the tobacco budworm moth *Heliothis virescens*: specified subdivision in four compartments according to information about biologically significant compounds. J Comp Physiol A 183:669–682.

Bjaalie JG, Brodal P. 1989. Visual pathways to the cerebellum: segregation in the pontine nuclei of terminal fields from different visual cortical areas in the cat. Neurosci 29:95–107.

Bjaalie JG, Brodal P. 1997. Cat pontocerebellar network: numerical capacity and axonal collateral branching of neurones in the pontine nuclei projecting to individual paraflocular folia. Neurosci Res 27: 199–210.

Bjaalie JG, Daehlen M, Stensby TV. 1997a. Surface modelling from biomedical data. In: Daehlen M, Tveito A, editors. Numerical methods and software tools in industrial mathematics. Boston: Birkhauser. p 9–26.

Bjaalie JG, Sudbø J, Brodal P. 1997b. Corticopontine terminal fibres form small scale clusters and large scale lamellae in the cat. Neuroreport 8:1651–1655.

Bolz J, Novak N, Götz M, Bonhoeffer T. 1990. Formation of target-specific neuronal projections in organotypic slice cultures from rat visual cortex. Nature 346:359–362.

Bolz J, Novak N, Staiger V. 1992. Formation of specific afferent connections in organotypic slice cultures from rat visual cortex co-cultured with lateral geniculate nucleus. J Neurosci 12:3054–3070.

Bolz J, Götz M, Hubener M, Novak N. 1993. Reconstructing cortical connections in a dish. Trends Neurosci 16:310–316.

Bower JM. 1997. Is the cerebellum sensory for motor's sake, or motor for sensory's sake: the view from the whiskers of a rat? Progr Brain Res 114:463–96.

Bower JM, Kassel J. 1990. Variability in tactile projection patterns to cerebellar folia crus IIA of the Norway rat. J Comp Neurol 302:768–778.

Bower JM, Beermann DH, Gibson JM, Shambes GM, Welker W. 1981. Principles of organization of a cerebro-cerebellar circuit. Micromapping the projections from cerebral (SI) to cerebellar (granule cell layer) tactile areas of rats. Brain Behav Evol 18:1–18.

Brodal P. 1968. The corticopontine projection in the cat. I. Demonstration of a somatotopically organized projection from the primary sensorimotor cortex. Exp Brain Res 5:210–234.

Brodal P. 1978. The corticopontine projection in the rhesus monkey. Origin and principles of organization. Brain 101:251–283.

Brodal P. 1987. Organization of cerebropontocerebellar connections as studied with anterograde and retrograde transport of HRP-WGA in the cat. In: King JS, editor. New concepts in cerebellar neurobiology. New York: Alan R. Liss, Inc. p 151–182.

Brodal P, Bjaalie JG. 1992. Organization of the pontine nuclei. Neurosci Res 13:83–118.

Brodal P, Bjaalie JG. 1997. Salient anatomic features of the cortico-pontocerebellar pathway. Progr Brain Res 114:227–249.

Brodal P, Bjaalie JG, Aas J-E. 1991. Organization of cingulo-pontocerebellar connections in the cat. Anat Embryol 184:245–254.

Burne RA, Mihailoff GA, Woodward DJ. 1978. Visual corticopontine input to the paraflocculus: a combined autoradiographic and horseradish peroxidase study. Brain Res 143:139–146.

Chapin JK, Lin CS. 1984. Mapping the body representation in the SI cortex of anesthetized and awake rats. J Comp Neurol 229:199–213.

Chapin JK, Lin CS. 1990. The somatic sensory cortex of the rat. In: Kolb B, Tees RC, editors. The cerebral cortex of the rat. Cambridge, MA: MIT Press. p 341–380.

De Carlos JA, O'Leary DD. 1992. Growth and targeting of subplate axons and establishment of major cortical pathways. J Neurosci 12:1194–1211.

Erzurumlu RS, Jhaveri S. 1992. Emergence of connectivity in the embryonic rat parietal cortex. Cereb Cortex 2:336–352.

Fabri M, Burton H. 1991. Topography of connections between primary somatosensory cortex and posterior complex in rat: a multiple fluorescent tracer study. Brain Res 538:351–357.

Geiger B. 1993. Three-dimensional modelling of human organs and its application to diagnosis and surgical planning, report 2105. Sophia-Antipolis, France: Institut National de Recherche en Informatique et en Automatique.

Gerfen CR, Sawchenko PE. 1984. An anterograde neuroanatomical tracing method that shows the detailed morphology of neurons, their axons and terminals: immunohistochemical localization of an axonally transported plant lectin, *Phaseolus vulgaris* leucoagglutinin (PHA-L). Brain Res 290:219–238.

Gonzales L, Shumway C, Morissette J, Bower JM. 1993. Developmental plasticity in cerebellar tactile maps: fractured maps retain fractured organization. J Comp Neurol 332:487–498.

Götz M, Novak N, Bastmeyer M, Bolz J. 1992. Membrane bound molecules in rat cerebral cortex regulate thalamic innervation. Development 116: 507–519.

Gribnau AA, de Kort EJ, Dederen PJ, Nieuwenhuys R. 1986. On the development of the pyramidal tract in the rat. II. An anterograde tracer study of the outgrowth of the corticospinal fibers. Anat Embryol (Berlin) 175:101–110.

Heffner CD, Lumsden AG, O'Leary DD. 1990. Target control of collateral extension and directional axon growth in the mammalian brain. Science 247:217–220.

Hicks SP, D'Amato CJ. 1968. Cell migrations to the isocortex in the rat. Anat Rec 160:619–634.

Joosten EA, van der Ven PF, Hooiveld MH, ten Donkelaar HJ. 1991. Induction of corticospinal target finding by release of a diffusible, chemotropic factor in cervical spinal grey matter. Neurosci Lett 128: 25–28.

Joosten EA, Bar PR, Gispen WH, Bregman BS. 1993. Transient projections from rat occipital cortex are able to respond to a spinal target derived diffusible factor in vitro. Neurosci Lett 164:85–88.

Joosten EA, Gispen WH, Bar PR. 1994. Tropism and corticospinal target selection in the rat. Neuroscience 59:33–41.

Kincaid AE, Zheng T, Wilson CJ. 1998. Connectivity and convergence of single corticostriatal axons. J Neurosci 18:4722–4731.

Koralek KA, Olavarria J, Killackey HP. 1990. Areal and laminar organization of corticocortical projections in the rat somatosensory cortex. J Comp Neurol 299:133–150.

Kosinski RJ, Neafsey EJ, Castro AJ. 1986. A comparative topographical analysis of dorsal column nuclear and cerebral cortical projections to the basilar pontine gray in rats. J Comp Neurol 244:163–173.

Kosinski RJ, Azizi SA, Mihailoff GA. 1988. Convergence of cortico- and

cuneopontine projections onto components of the pontocerebellar system in the rat: an anatomical and electrophysiological study. Exp Brain Res 71:541–556.

Lanciego JL, Wouterlood FG. 1994. Dual anterograde axonal tracing with *Phaseolus vulgaris*-leucoagglutinin (PHA-L) and biotinylated dextran amine (BDA). Neurosci Protocols 94-050-06-01-13.

Lee HS, Mihailoff GA. 1990. Convergence of cortical and cerebellar projections on single basilar pontine neurons: a light and electron microscopic study in the rat. Neuroscience 39:561–577.

Leergaard TB, Bjaalie JG. 1995. Semi-automatic data acquisition for quantitative neuroanatomy. MicroTrace—computer programme for recording of the spatial distribution of neuronal populations. Neurosci Res 22:231–243.

Leergaard TB, Bjaalie JG. 1998. From cortical 2-D to brain stem 3-D maps: organization of corticopontine projections in developing and adult rats. Soc Neurosci Abstr 24:262.9.

Leergaard TB, Lakke EA, Bjaalie JG. 1995. Topographical organization in the early postnatal corticopontine projection: a carbocyanine dye and 3-D computer reconstruction study in the rat. J Comp Neurol 361:77–94.

Lehre KP, Levy LM, Ottersen OP, Storm-Mathisen J, Danbolt NC. 1995. Differential expression of two glial glutamate transporters in the rat brain: quantitative and immunocytochemical observations. J Neurosci 15:1835–1853.

Lyngstad KA, Thompson JH, Bower JM, Bjaalie JG. 1996. Somatosensory pathways to the cerebellum: spatial organization of electrophysiologically identified corticopontine terminal fibres in the rat. Soc Neurosci Abstr 21:467.12.

Malmierca MS, Rees A, Le Beau FE, Bjaalie JG. 1995. Laminar organization of frequency-defined local axons within and between the inferior colliculi of the guinea pig. J Comp Neurol 357:124–144.

Malmierca MS, Leergaard TB, Bajo VM, Bjaalie JG, Merchan MA. 1998. Anatomic evidence of a three-dimensional mosaic pattern of tonotopic organization in the ventral complex of the lateral lemniscus in cat. J Neurosci 18:10603–10618.

McCandlish CA, Li CX, Waters RS. 1993. Early development of the SI cortical barrel field representation in neonatal rats follows a lateral-to-medial gradient: an electrophysiological study. Exp Brain Res 92: 369–374.

Mesulam M-M. 1982. Principles of horseradish peroxidase neurohistochemistry and their applications for tracing neural pathways - axonal transport, enzyme histochemistry and light microscopic analysis. In: Mesulam M-M, editor. Tracing neural connections with horseradish peroxidase. Chichester: John Wiley & Sons. p 1–151.

Mihailoff GA. 1995. Orthograde axonal transport studies of projections from the zona incerta and pretectum to the basilar pontine nuclei in the rat. J Comp Neurol 360:301–318.

Mihailoff GA, Burne RA, Woodward DJ. 1978. Projections of sensorimotor cortex to the basilar pontine nuclei in the rat: an autoradiographic study. Brain Res 145:347–354.

Mihailoff GA, McArdle CB, Adams CE. 1981. The cytoarchitecture, cytology, and synaptic organization of the basilar pontine nuclei in the rat. I. Nissl and Golgi studies. J Comp Neurol 195:181–201.

Mihailoff GA, Adams CE, Woodward DJ. 1984. An autoradiographic study of the postnatal development of sensorimotor and visual components of the corticopontine system. J Comp Neurol 222:116–127.

Mihailoff GA, Lee H, Watt CB, Yates R. 1985. Projections to the basilar pontine nuclei from face sensory and motor regions of the cerebral cortex in the rat. J Comp Neurol 237:251–263.

Mihailoff GA, Kosinski RJ, Azizi SA, Border BG. 1989. Survey of noncortical afferent projections to the basilar pontine nuclei: a retrograde tracing study in the rat. J Comp Neurol 282:617–643.

Mihailoff GA, Kosinski RJ, Azizi SA, Lee HS, Border BG. 1992. The expanding role of the basilar pontine nuclei as a source of cerebellar afferents. In: Llinas R, Sotelo C, editors. The cerebellum revisited. New York: Springer-Verlag. p 135–164.

Miller MW. 1987. Effect of prenatal exposure to alcohol on the distribution and time of origin of corticospinal neurons in the rat. J Comp Neurol 257:372–382.

Novak N, Bolz J. 1993 Formation of specific efferent connections in organotypic slice cultures from rat visual cortex cocultured with lateral geniculate nucleus and superior colliculus. Eur J Neurosci 5:15–24.

O'Leary DD, Terashima T. 1988. Cortical axons branch to multiple subcortical targets by interstitial axon budding: implications for target recognition and "waiting periods." Neuron 1:901–910.

O'Leary DD, Heffner CD, Kutka L, Lopez-Mascaraque L, Missias A, Reinoso BS. 1991. A target-derived chemoattractant controls the development of the corticopontine projection by a novel mechanism of axon targeting. Development 2(Suppl):123–130.

Panto MR, Cicirata F, Angaut P, Parenti R, Serapide F. 1995. The projection from the primary motor and somatic sensory cortex to the basilar pontine nuclei. A detailed electrophysiological and anatomical study in the rat. J Hirnforsch 36:7–19.

Potter RF, Rüegg DG, Wiesendanger M. 1978. Responses of neurones of the pontine nuclei to stimulation of the sensorimotor, visual and auditory cortex of rats. Brain Res Bull 3:15–19.

Rüegg D, Wiesendanger M. 1975. Corticofugal effects from sensorimotor area I and somatosensory area II on neurones of the pontine nuclei in the cat. J Physiol (London) 247:745–757.

Rüegg DG, Sequin JJ, Wiesendanger M. 1977. Effects of electrical stimulation of somatosensory and motor areas of the cerebral cortex on neurons of the pontine nuclei in squirrel monkeys. Neuroscience 2:923–927.

Schmahmann JD, Pandya DN. 1997. The cerebrocerebellar system. Int Rev Neurobiol 41:31–60.

Schwarz C, Thier P. 1995. Modular organization of the pontine nuclei: dendritic fields of identified pontine projection neurons in the rat respect the borders of cortical afferent fields. J Neurosci 15:3475–3489.

Schwarz C, Thier P. 1996. Comparison of projection neurons in the pontine nuclei and the nucleus reticularis tegmenti pontis of the rat. J Comp Neurol 376:403–419.

Shambes GM, Gibson JM, Welker W. 1978. Fractured somatotopy in granule cell tactile areas of rat cerebellar hemispheres revealed by micromapping. Brain Behav Evol 15:94–140.

Shumway C, Morissette J, Gruen P, Bower JM. 1999. Plasticity in cerebellar tactile maps in the adult rat. J Comp Neurol 413:583–592.

Smart IH. 1984. Histogenesis of the mesocortical area of the mouse telencephalon. J Anat 138:537–552.

Suzuki DA, May JG, Keller EL, Yee RD. 1990. Visual motion response properties of neurons in dorsolateral pontine nucleus of alert monkey. J Neurophysiol 63:37–59.

Thier P, Koehler W, Buettner UW. 1988. Neuronal activity in the dorsolateral pontine nucleus of the alert monkey modulated by visual stimuli and eye movements. Exp Brain Res 70:496–512.

Tomasch J. 1968. The overall information carrying capacity of the major afferent and efferent cerebellar cell and fiber systems. Confin Neurol 30:359–367.

Tomasch J. 1969. The numerical capacity of the human cortico-pontocerebellar system. Brain Res 13:476–484.

Torigoe Y, Blanks RH, Precht W. 1986. Anatomical studies on the nucleus reticularis tegmenti pontis in the pigmented rat. II. Subcortical afferents demonstrated by the retrograde transport of horseradish peroxidate. J Comp Neurol 243:88–105.

Vassbø K, Nicotra G, Wiberg M, Bjaalie JG. 1999. Monkey somatosensory cerebrocerebellar pathways: uneven densities of corticopontine neurons in different body representations of areas 3b, 1, and 2. J Comp Neurol 406:109–128.

Welker C. 1971. Microelectrode delineation of fine grain somatotopic organization of (SmI) cerebral neocortex in albino rat. Brain Res 26:259–275.

Welker C. 1976. Receptive fields of barrels in the somatosensory neocortex of the rat. J Comp Neurol 166:173–189.

Welker W. 1987. Spatial organization of somatosensory projections to granule cell cerebellar cortex: functional and connectional implications of fractured somatotopy (summary of Wisconsin studies). In: King JS, editor. New concepts in cerebellar neurobiology. New York: Alan R. Liss. p 239–280.

Wiesendanger R, Wiesendanger M. 1982. The corticopontine system in the rat. II. The projection pattern. J Comp Neurol 208:227–238.

Woelcke M. 1942. Eine neue Methode der Markscheidenfarbung. J Psychol Neurol 51:199–202.

Woolsey CN. 1958. Organization of somatic sensory and motor areas of the cerebral cortex. In: Harlow HF, Woolsey CN, editors. Biological and biochemical bases of behavior. Madison, WI: University of Wisconsin Press. p 63–81.

Woolston DC, Kassel J, Gibson JM. 1981. Trigeminocerebellar mossy fiber branching to granule cell layer patches in the rat cerebellum. Brain Res 209:255–269.